Design, Manufacturing and Testing of an Environmentally-Green Bipropellant Thruster

A Senior Project

presented to

The Faculty of the Aerospace Engineering Department

California Polytechnic State University, San Luis Obispo

In Partial Fulfillment

Of the Requirements for the Degree

Bachelor of Science

By

Alex Bendoyro, Gabriel Sanchez, Erin Stearns, and Phillip Takahashi

June 2011

Design, Manufacturing and Testing of an Environmentally-Green Bipropellant Thruster

Alex Bendoyro[1], Gabriel Sanchez[2], Erin Stearns[3], and Phillip Takahashi[4]
California Polytechnic State University, San Luis Obispo, CA, 93407

Approved by

Dr. Kristina Jameson[5]
California Polytechnic State University, San Luis Obispo, CA, 93407

This project reviews the design, manufacturing and experimentation process of a green bi-propellant thruster designed to output 5 lbf. The goals were to successfully design, manufacture and test a thruster, while discovering the complications that arise through out the complete design process of a green thruster. The thruster was successfully designed using ideal rocket equations and the design was successfully confirmed using CFD and FEA. Manufacturing of the thruster was fully planned and revealed mild flaws in thruster design. For example some features were not manufacturable to the exact measurements desired. Testing of the engine gave results inconsistent with expected values with a maximum nominal thrust of 2.38 lbf. Measurement errors in thrust and mass flow rates caused calculations of thruster performance, such as ISP, to vary from expected values. Measurement errors are suspected to stem from a combination of incorrect ideal assumptions and test bed design flaws.

Nomenclature

A	=	pipe area
CFD	=	computational fluid dynamics
D	=	diameter
F	=	load cell force
F	=	Fahrenheit
f	=	freud number
FEA	=	finite element analysis
$F_{measured}$	=	measured nominal thruster force
ft	=	feet
F_{tare}	=	measured initial load cell force
g	=	gravitational acceleration
in.	=	inches
ISP	=	specific impulse
L	=	length
$\dot{m}$	=	individual mass flow rate

[1] Undergraduate Student, Aerospace Engineering Department, 1 Grand Avenue.
[2] Undergraduate Student, Aerospace Engineering Department, 1 Grand Avenue.
[3] Undergraduate Student, Aerospace Engineering Department, AIAA Student Member.
[4] Undergraduate Student, Aerospace Engineering Department, 1 Grand Avenue.
[5] Professor, Aerospace Engineering Department, 1 Grand Avenue, AIAA Member.

$\dot{m}_{tot}$ = combined mass flow rate
M = Mach number
P = gas line pressure
P = thruster chamber pressure
psi = pound per square inch
psia = pound per square inch, actual
psig = pound per square inch, gauge
P1 = regulator pressure
r = internal radius
R = gas constant for oxygen or hydrogen
R = Rankine
RG = percent or ratio of hydrogen or oxygen mass flow
s = seconds
t = thickness
T = temperature or thrust
V_{LC} = measured load cell potential
V_{PT} = measured pressure transducer potential
γ = ratio of specific heats
ρ = density
σ = stress

I. Introduction

SPACECRAFT propulsion relies heavily on the usage of extremely toxic propellants, including carcinogenic hydrazine. These hazardous materials have proven to be the most performance effective when it comes to spacecraft propulsion systems thanks to their high ISPs, making them the most widely used in industry. However, with such toxic propellants come many difficulties and restrictions, leading to opportunities for new developments. Less hazardous propellants are starting to become relevant and are being considered in the spacecraft propulsion realm. These hazardous materials will be safer and considered, "green" options for spacecraft. These green propellants would prove to be more cost-effective due to the elimination for the current special handling, such as hazardous material suits and extensive safety procedures, with both the general usage and transportation. They would also provide a safer work environment and eliminate a lot of the risk that personnel are exposed to who work with these propellants. However, at this time, no green propellants have been found to consistently perform as effectively as their toxic competitors.

Bipropellant thrusters are not a unique concept and are widely used aerospace applications today. For example satellites use thrusters for attitude control such as the Astrium S10[1] seen in Fig. 1. Launch vehicles can use bipropellant engines in their main thrusters like the Delta IV's second stage RL10 engine made by Pratt and Whitney[2] seen in Fig. 2. However, the use of green fuels in a bipropellant is far less common. Typical fuels and oxidizers include mono-methyl-hydrazine (MMH), di-nitrogen-tetroxide (N_2O_4), Rocket Propellant-1 (RP-1) and unsymmetrical di-methyl-hydrazine (UDMH), none of which are safely handle-able by people. These fuels are toxic by themselves and produce toxic byproducts when they combust. Green bi-propellants have the advantage of being relatively easy to handle and non-toxic to humans and the environment whether in their initial state or after combustion. Recent advances in social and technological philosophies have pushed for a move to a green future and so it is important to research the technology to keep industry with the times.

This report reviews the process of designing, manufacturing and testing a student designed green bipropellant thruster. This thruster is designed to use environmentally safe propellants while providing a minimum thrust of five pounds. This project presented challenges particularly in the form of design, manufacturing, safety and budgeting. It was with the responsibility of creating a green future that this project was born. The overall goals of this project are to design, manufacture and test a green bipropellant thruster and to understand the issues that go with manufacturing and testing a thruster.

Figure 1: This is a picture of Astrium S10 thruster. It is a 10 N thruster used for satellite attitude control and has even been used in groups for orbital transfers

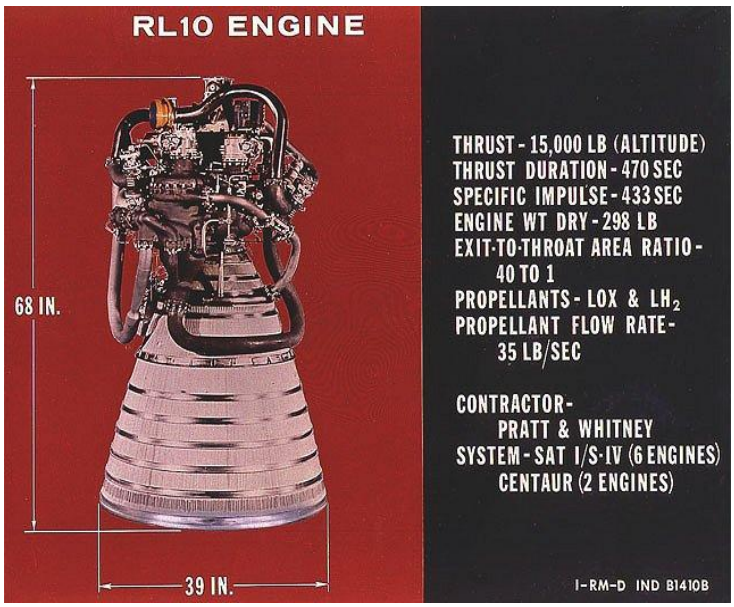

Figure 2: This is a picture of Pratt and Whitney's RL10 bipropellant engine. It is used in the second stage of the Delta IV Heavy.

II. Design Process

The design process for the bipropellant thruster can be broken down into several separate aspects. This includes the propellant selection, material selection, thruster sizing and modeling. Variables in these select areas were constantly being considered and traded throughout the design period to ensure that the chosen design would be robust, consistent and safe.

A. Propellant Selection

The fuel selection began by gathering several readily available bipropellant fuel combinations then narrowing down the list based on cost, safety, availability, and environmental impact. Hydrogen, oxygen, hydrogen peroxide and alkanes like propane and methane were considered although they release of trace amounts of carbon dioxide during combustion. Table 1 provides a list of fuels and oxidizers considered for this project[3,4,5,6]. Liquid Oxygen and hydrogen were removed immediately for their cryogenic state requirements, which would have greatly increased cost and risk in the form of storability. To further reduce options, it was determined that gaseous fuels and oxidizers would greatly simplify thruster design by eliminating the need for an atomizer. Options were further reduced by considering what equipment was already available for use in the Cal poly Aerospace labs to help attenuate cost. Gaseous hydrogen and oxygen were chosen as the optimal propellants for this experiment because they meet the requirements of green propellants, are relatively inexpensive, are easy obtain and there was already equipment in place and available for use.

Table 1. This table shows the list of considered fuels and oxidizers

Oxidizers	Fuel
Oxygen	Hydrogen
Nitrous Dioxide	Propane
Dihydrogen Dioxide	Kerosene
Ammonium Dinitramide	Methane
	Ethanol

B. Material Selection

Research was performed to determine the appropriate components and materials needed to safely design and test our thruster. Factors used to determine this included how resistant the materials are to heat, corrosion, oxygen embrittlement, hydrogen embrittlement and forces resulting from thrust or pressure in the system. The two materials with these properties that stand out are graphite and stainless steel. Both materials are comparable in price for a foot-long cylinder, so budgetary concerns for material acquisition was not a deciding factor in selection. Stainless steel is a very hard material that can be more difficult to machine. However, graphite has a difference set of issues in manufacturing process due to the carbon dust it creates during the machining process. Graphite also does not have as high of a thermal capacity as steel.

Another factor that needed to be considered was the actual process of manufacturing. Due to the lack of applied manufacturing process experience, it was determined that a test build would be beneficial to help identify manufacturing issues that could not be predicted. An alternative metal was chosen to allow for an inexpensive dry run of the manufacturing process aluminum. This aluminum thruster was ultimately used for manufacturing process practice and ignition testing. The ignition testing consisted of mounting the test chamber without the nozzle and experimenting with rocket igniters and spark plugs at various mixture ratios and pressures. The primary advantage of this test was to determine if spark plugs were a reliable and robust form of ignition, as the rocket igniters were already a proven method, without risking drilling and tapping an unnecessary hole into the real thruster.

C. **Initial Calculations and Thruster Sizing**

Thruster design and sizing consisted of several considerations; primarily exit velocity, exit pressure, chamber pressure and chamber/nozzle diameter. Exit velocity and pressure were important because these two values determine the amount of thrust the engine would produce. Chamber pressure was important as it affected the required strengths of the thruster (IE wall thickness) and components such as valves and piping. Chamber and nozzle diameters were important for the sake of manufacturing capabilities. The primary issue with a thruster design of this caliber was making it large enough that it would be manufacturable given the production methods available to the team, but small enough to meet the goal of 5 lbf of thrust.

Sizing started with the ideal rocket equations seen in Eq.s 1-9,

$$A_e = A_r\left(\frac{\gamma+1}{2}\right)^{\frac{-(\gamma+1)}{2(\gamma+1)}} \frac{\left(1+\frac{\gamma-1}{2}M_e{}^2\right)^{\frac{\gamma+1}{2(\gamma-1)}}}{M_e} \tag{1}$$

$$P_t = \frac{P_e}{\left(1+\frac{\gamma-1}{2}M_e{}^2\right)^{\frac{-\gamma}{\gamma-1}}} \tag{2}$$

$$P_c = \frac{P_t}{\left(1+\frac{\gamma-1}{2}\right)^{\frac{-\gamma}{\gamma-1}}} \tag{3}$$

$$T_t = \frac{T_c}{\left(1+\frac{\gamma-1}{2}\right)} \tag{4}$$

$$T_e = T_t\left(1+\frac{\gamma-1}{2}M_e{}^2\right)^{-1} \tag{5}$$

$$V_e = M_e\sqrt{\gamma R T_e} \tag{6}$$

$$\dot{m} = \frac{A_t P_t}{\sqrt{T_r}}\sqrt{\frac{\gamma}{R}}\left(\frac{\gamma+1}{2}\right)^{\frac{-(\gamma+1)}{2(\gamma-1)}} \tag{7}$$

$$F = \dot{m}V_e + (P_e - P_a)A_e \tag{8}$$

$$ISP = \frac{F}{\dot{m}g} \tag{9}$$

where A is the area at the indicated station in ft^2, γ is ratio of specific heats of the exhaust gasses, M is mach number at the given station, P is pressure in psfa at the given station, R is the gas constant of the exhaust gas in ft-lbf/slug-R,

V is gas velocity at the given station in ft/s, T is temperature at the given station in R, m is mass flow in slugs/s, F is thrust in lbf, g is gravity in ft/s^2 and ISP is specific impulse in s. Knowing that the desired force was 5 lbf, ideal combustion temperature of hydrogen and oxygen is 5326 R[3], the ratio of specific heat for a hydrogen-oxygen reaction is 1.26[3] and that ambient conditions would be approximately that of STP, the values left to decide were throat area, exit pressure and exit velocity. Key values in the ideal rocket equation such as ISP, exit area and chamber pressure were left to be solved for from the above values.

The first iteration of the thruster resulted in a chamber pressure of 260 psi, an ISP of 213.6 s, and an exit area of .0584 in^2 which had resulted from the selected values of an exit pressure of 14.7 psi, a throat area of 0.0276 in^2 and an exit velocity of mach 2.15. This first iteration was based on the idea of ideal expansion of the exhaust gases and the assumption that a thruster built around the afore-mentioned throat area could be reasonably constructed. However this first iteration was discarded for one main reason. The desired chamber pressure of 260 psi was not attainable using the pressure regulators available. New pressure regulators could have been purchased but the funds were not within the given project budget. Due to this fact, a second design iteration had to be considered.

The second iteration of the thruster resulted in a chamber pressure of 120 psi, an ISP of 176.63 s, and an exit area of 0.073 in^2 which had resulted from the selected values of an exit pressure of 29.4 psi, a throat area of 0.0707 in^2 and an exit velocity of Mach 1.2. This design was built around an under-expanded exhaust and an enlarged throat to allow increased mass flow. A combination of the enlarged throat, lowered exit mach and increased exit pressure allowed thrust to increase while simultaneously dropping chamber pressure. This design was decided to be acceptable for performance and manufacturing considerations. Other dimensions such as combustion chamber length, nozzle length and chamber length were determined using known relationships defined in Reference 1 and resulted in the design seen in Fig. 3 and Fig. 4.

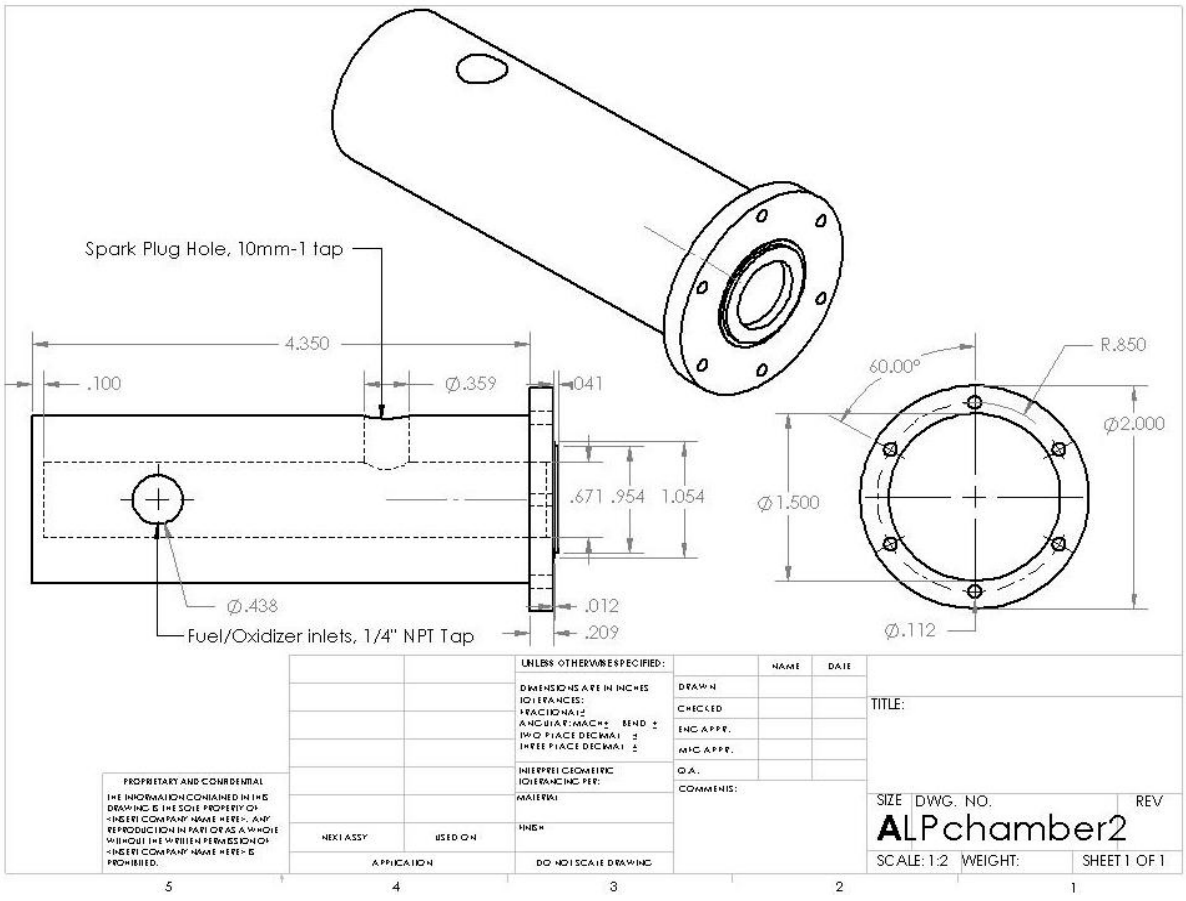

Figure 3: This drawing shows the full schematic of the combustion chamber with all important measurements

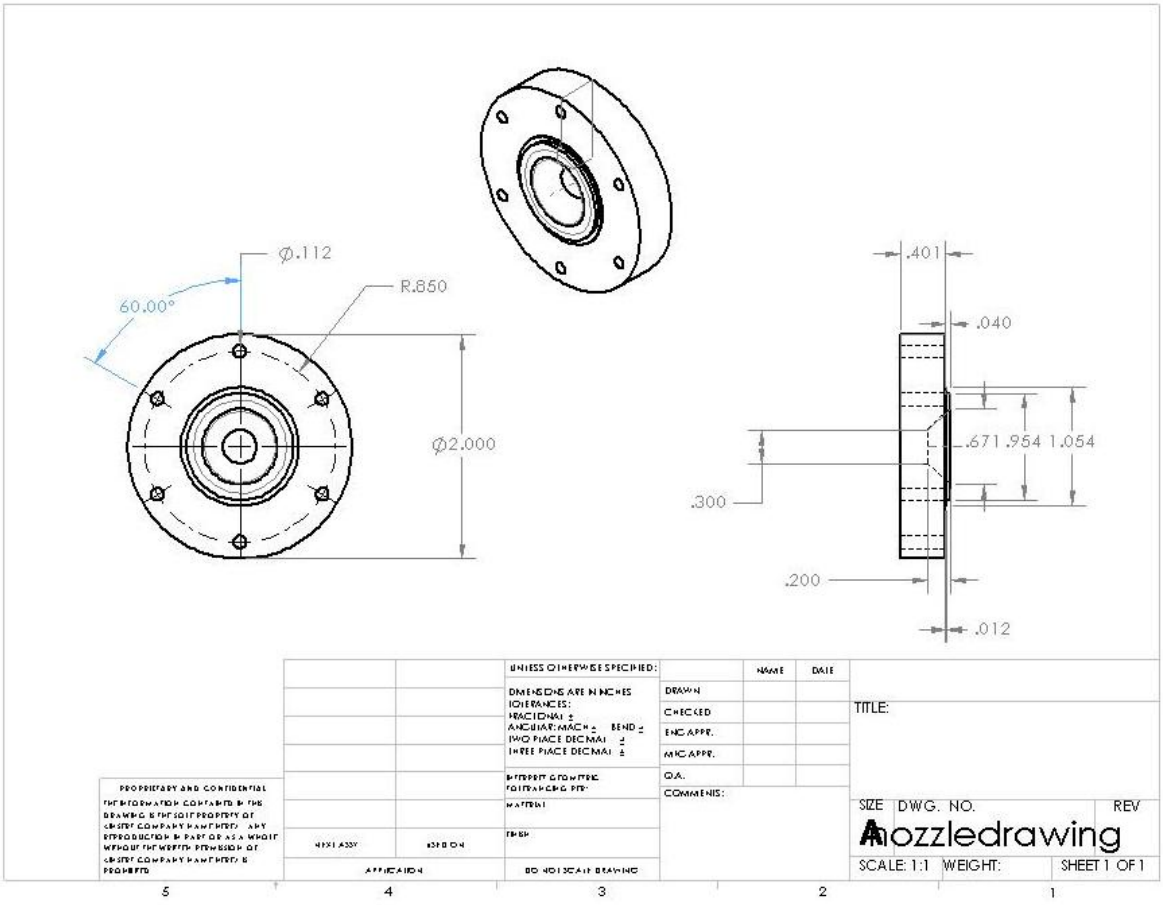

Figure 4: This drawing shows a full schematic of the thruster nozzle with all important dimensions.

With the thruster fully sized, components had to be sized. This was done by first determining the required mass flow for the oxygen and hydrogen. To determine the correct flow rates, the mixture ratio has to be calculated. Mixture ratio calculation begins with the stoichiometric balance of a hydrogen and oxygen combustion seen in Eq. 10,

$$2H_2 + O_2 = 2H_2O + 286\ kJ \tag{10}$$

This stoichiometric balance shows that 2 moles of hydrogen is required for each mole of oxygen. Converting moles to slugs, the ratio of fuel to oxygen comes to 0.125.

Knowing the desired fuel ratio and total mass flow, it was possible to properly calculate flow conditions. Knowing that the measured pipe inner diameter of the fuel and oxidizer lines were 0.19 in.and that density of the gasses at 120 psia was 0.00164 slugs/ft^3 and 0.0260 slugs/ft^3 for hydrogen and oxygen respectively, gas velocity in the pipes could be calculated using Eq. 11,

$$\mathrm{V} = \frac{\dot{\mathrm{m}}}{\rho \mathrm{A}} \mathrm{RG} \tag{11}$$

Where $\dot{m}$ is the total mass flow is slugs/s, ρ is the density of the respective gas in slugs/ft^3, A is the inside area of the pipe in ft^2, RG is the percent or ratio of the respective gas and V is gas velocity in ft/s. This equation resulted in a velocity of 69.3 ft/s for the hydrogen and 34.7 ft/s for the oxygen. With velocity calculated, head loss from tank to thruster inlet could be calculated using Eq. 12,

$$H = \frac{fLV^2}{2Dg} + \frac{kV^2}{2g} \tag{12}$$

where k is the minor loss coefficient for the pipe and is the sum of all piping impedances, which is unitless, g is acceleration due to gravity at sea level in ft/s^2, L is the value for the total length of the pipe in ft, D is the inner diameter of the pipe in ft, f is the friction factor of the pipe and H is the head loss in ft. For a 90 degree turn minor loss coefficient is 0.35, for a T-junction, k is 0.9 and for a needle valve, k is 2 which results in a total k of 5. The friction factor f for the pipe was found to be 0.15 for smooth piping. L was measured to be 5.84 ft and D was measured to be 0.19 in. Using these values, the head loss was calculated to be 4.27 feet for the hydrogen and 1.07 feet for the oxygen. Converting the head loss to pressure, the pressure loss was found to be 0.6385 psi for the hydrogen and 2.54 psi for the oxygen.

During the process of sizing the thruster some key relationships were discovered. The primary relationships were of exit Mach to exit pressure, exit mach to force, exit pressure to force and all the afore-mentioned to chamber pressure. It was a culmination of identifying these relationships that allowed the thruster to be designed. Increasing Mach was an option for adjusting thrust via the area ratio. The issue with increasing the Mach was that the chamber pressure increased and the exit pressure decreased which would typically lessen the return of increasing Mach number. Adjusting pressure had a linear relationship where increasing exit pressure increased force and chamber pressure and decreasing exit pressure decreased force and chamber pressure. What was seen for exit pressure was that it had an inverse relationship on nozzle area ratio relative to mach number. The interesting phenomenon here is the affects of exit mach and exit pressure on thruster efficiency. It was determined that the best way to increase efficiency was to make the exit pressure as large as possible while keeping the Mach number as small as possible without dropping below the critical value of one. However, because this thruster was not designed for efficiency but rather manufacturability and a thrust goal of 5 lbf, the design goals did not include efficiency optimization.

D. **Finite Element Analysis and Computational Fluid Dynamics**

The thruster combustion chamber must withstand the high pressure oxidizer ranges from 60 psig to 130 psig. In order to insure that the thickness of the combustion chamber can survive these pressure ranges, an analytical approach was taken to find a preliminary thickness. Using hoop stress, this is defined in Eq.1, to predict the principal stresses of the pressurized combustion chamber.

$$\sigma_P = \frac{Pr}{t} \tag{13}$$

The pressure inside the combustion chamber, P, and the radius of the cylindrical pressure vessel, r, is calculated from the previous equations when finding the optimal thrust. The principle stress, σ_p, of the material is given by the manufactures of the aluminum rod and the steel rod which were 64 psi and 85 psi respectively. However, due to the fact that the aluminum thruster would be fired at the lower pressure range then aluminum would be sized according to the thickness of the steel combustion chamber. With a factor of safety of ten applied to the equation above, the minimum thickness the chamber needed to be is 0.005 in. However, this preliminary analysis does not take into consideration the thermal stress and the unique geometry of the entire thruster. Therefore, a numerical approach is needed to needed to justify the thickness that is needed for the thruster.

To confirm hand calculations, several computational fluid dynamics (CFD) and finite element analysis (FEA) models were made using material properties from the manufacturer. Figure 5 shows the FEA model of the thruster being deflected and illustrates that the thruster can withstand a pressure well in excess of 130 psia. The FEA model was tested using the numerical solver program Nastran[7]. Patran[7] was the pre-solver software. The FEA analysis indicates that the maximum deflection of a 0.1 in. thick wall would be 1.46 x 10^{-4} inches. This deflection would occur towards the exit nozzle area and less deflection would occur where the thruster is being supported in the middle. To consider whether this deflection is acceptable, the stress values on the combustion chamber were examined.

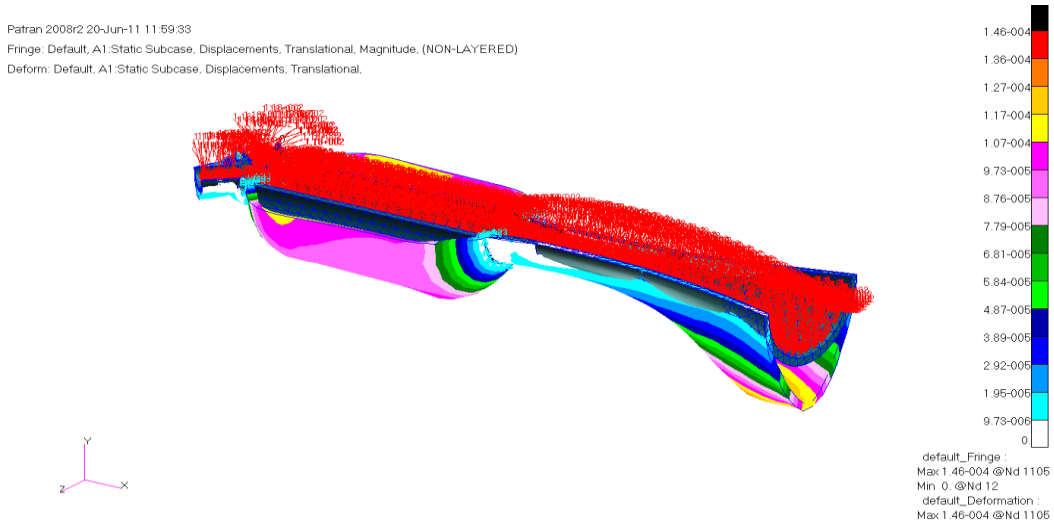

Figure 5: Patran/Nastran numerical calculation of the deflection the first iteration thruster will experience shows no dangerous deflections or strain concentration points.

The next FEA model that was produced during the analysis was the stress model. Figure 6 shows where the maximum stress locations are and various stress concentration throughout the model. One noticeable feature of the stress in the thruster is the location of the maximum stress of 1800 psi occurs in the combustion chamber, which is well below the yield stress of steel, even when greatly heated. Other parts of the thruster will also experiences heats in excess of 5000 R, which will increase the overall stress of the steel, but are still well within the yield strength of 316 stainless steel.

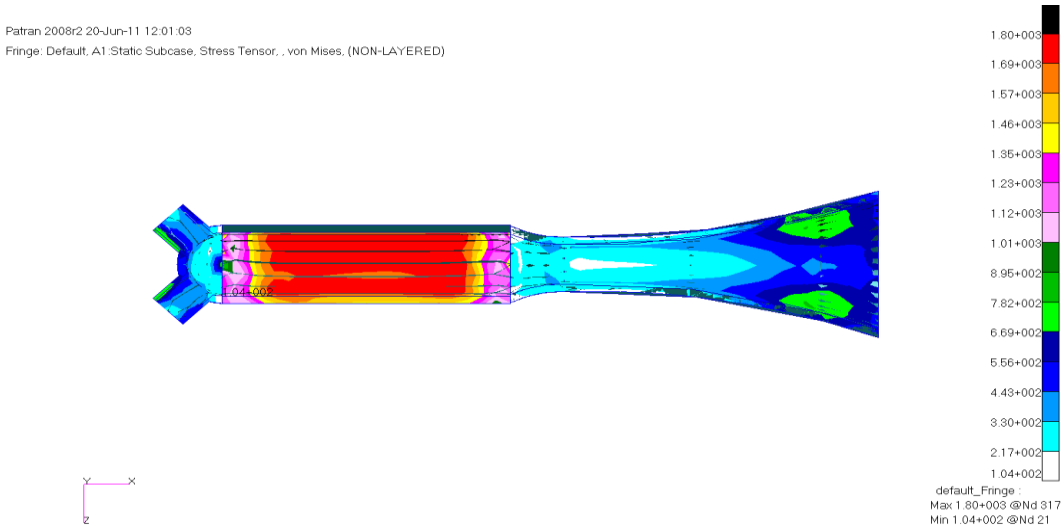

Figure 6: Patran/Nastran numerical calculation of the stresses the thruster will experience show a large margin of safety for this thruster iteration which is thinner than the final iteration.

The final iteration for the thruster had a combustion chamber thickness of 0.41 inches so there was no need to run another finite analysis. However there was a concern of the shear force the bolts would experience. Figure 7 illustrates the FEA analysis of the deflection a 1000 lb bolt load applied to the end of the combustion portion of the thruster. The maximum deflection the thruster was 0.0013 inches on the tips of where the bolt was to be fastened to.

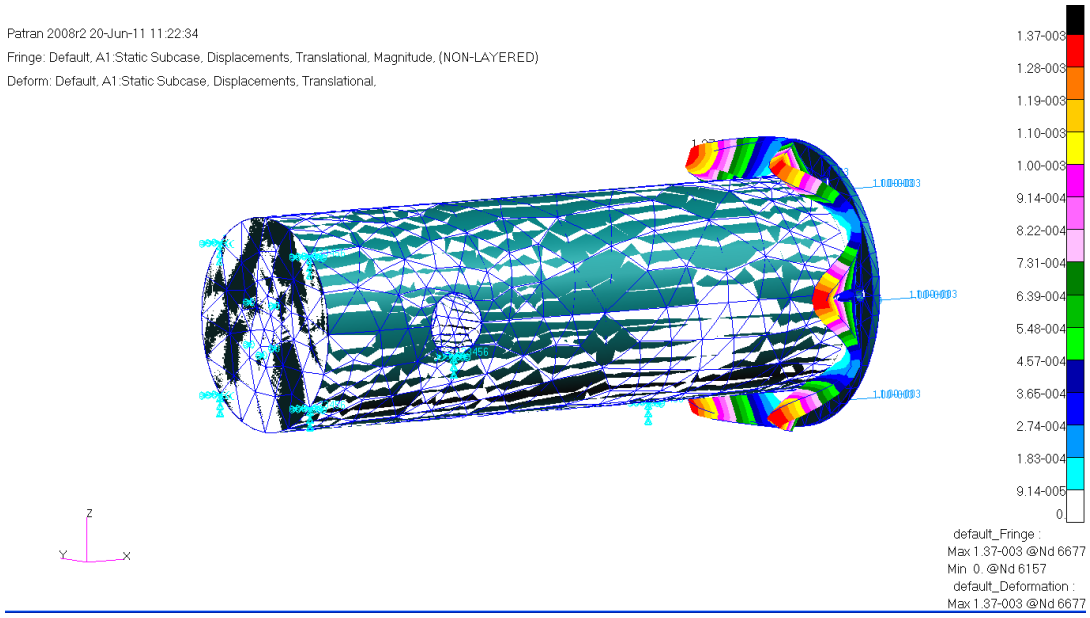

Figure 7: Patran/Nastran numerical calculation of the deflection due to the bolt load and indicate that there will be no problems from the bolts flexing.

To determine whether the deflection of the bolt load affected the structure, the stresses were then analyzed. The illustration of the FEA model stresses is depicted in Fig. 8 where high stress concentrations occur where holes have been drill through the structure. Each screw hole would experience a maximum stress of 52000 psi around the surface of the hole. For both aluminum and steel this stress is within the factor of safety with each having a margin of safety greater than 0.2. However, the 1000 lb bolt load has a factor of safety of 8 resulting in a final factor of safety of 8.2.

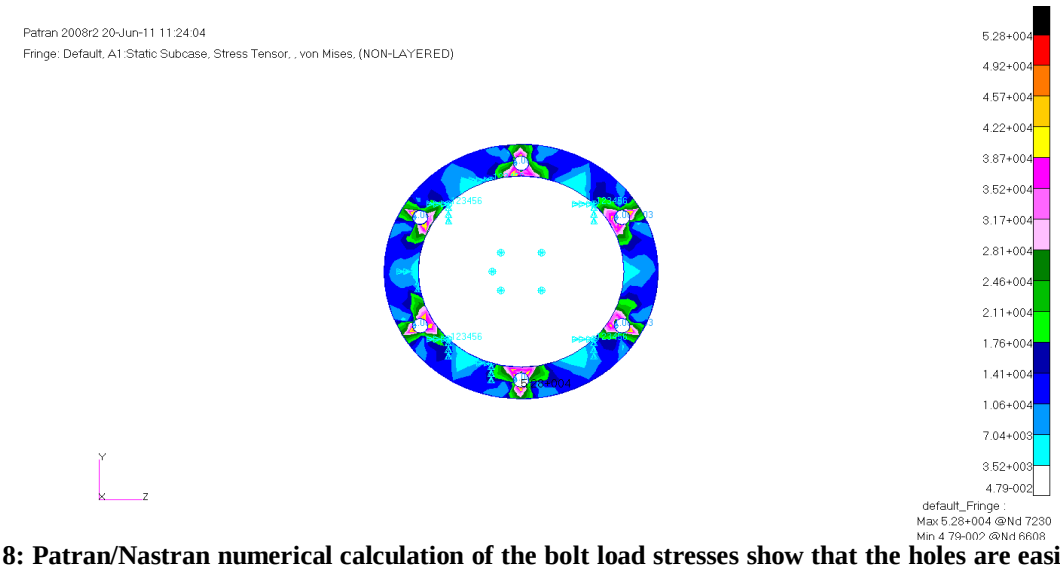

Figure 8: Patran/Nastran numerical calculation of the bolt load stresses show that the holes are easily able to withstand bolt flex.

CFD was used to check the calculated mass flow rate and the velocity of the flow of the thruster outlet. Using FloWorks application, in SolidWorks 2007, a numerical analysis was performed on the green-bi propellant thruster. Both gases introduced to the model had an initial pressure and temperature of 122 psi and 78 degrees Fahrenheit respectively. The outlet of the thruster had a final temperature of 78 degrees Fahrenheit and a final pressure of 14.7 psi. Figure 9 shows the velocity contour and trajectory of the gas motion inside the thruster. The

result of the CFD model shows that the exit velocity reached a value of 3914.5 ft/s with an average velocity of 391 ft/s inside the combustion chamber. However, it is important to know that the FlowWorks application does not take into consideration the combustion that is occurring inside the chamber that would cause both temperature and velocity would rise as a result of the chemical reaction. Knowing the exact pressure and velocity would require extensive research and program to determine the effects of the combustion would do to the gas particles inside the thruster. However, for this experiment the CFD model was used to give a rough estimate to the exit velocity and the path that the flow would travel. Therefore, a more precise model was not crucial for the experiment.

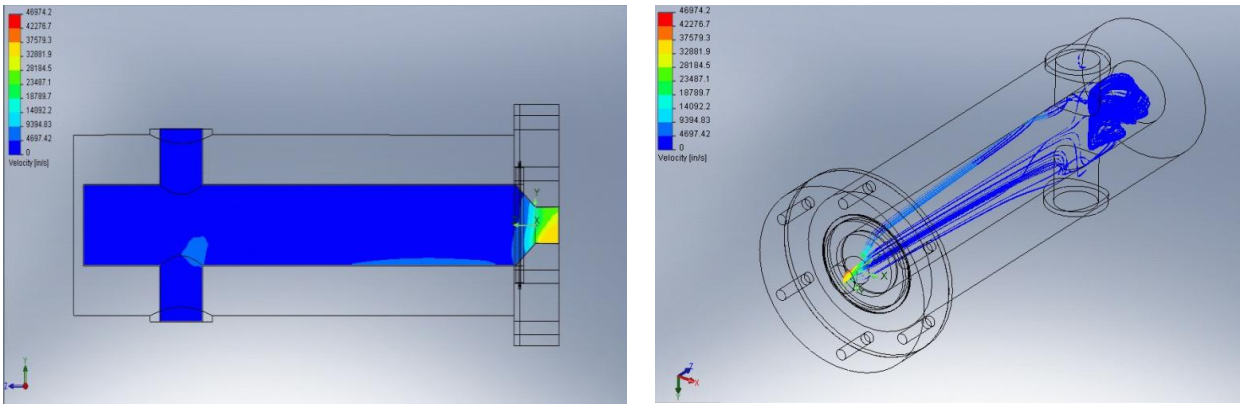

Figure 9: Velocity profile of the thruster using FloWorks. Results show similarities to hand calcs and indicate no unusual flow phenomena.

The CFD analysis also modeled the pressure decrease inside the thruster as the flow exited the nozzle. Figure 10 illustrates the static pressure contour and the trajectory of the gas motion inside the thruster. The result of the CFD model shows that the exit static pressure reached ambient pressure with an average static pressure inside the combustion chamber having 122.34 psi. One noticeable feature of both the pressure and velocity profiles show that flow travels in two distinct directions once it enters the chamber. Half of the flow travels towards the exit of the nozzle while the remainder of the flow backfilling to the remainder of the chamber. It was expected that the camber would be filled before escaping the nozzle, but the movement of the gas was unknown. This flow representation show to an extent what the flow will do while in the combustion chamber and the velocities it will create. However, from the CFD model, the exit velocity of 3914.5 ft/s is very similar to the calculated velocity flow that is discussed in greater depth in the analysis section.

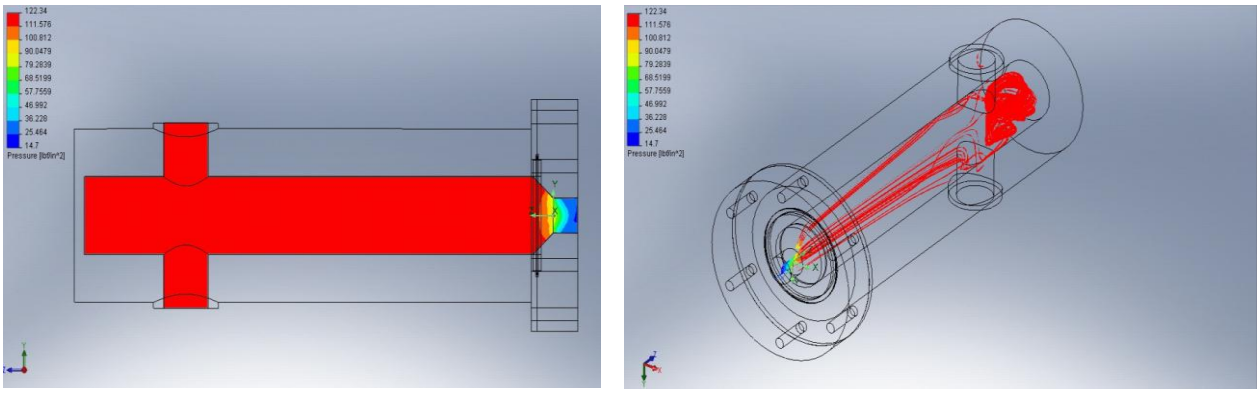

Figure 10: Pressure profile of the Thruster using FloWorks shows appropriate pressure decrease through the nozzle but unfortunately cannot show pressure concentration or fluctuation due to combustion.

By comparing the CFD result to analytical calculations, these findings concluded that the results of all computer models reasonably agreed with hand calculations; having a 12 % difference between the numerical and analytical values. The velocities of the inlet and outlet of the nozzle were analytically calculated by knowing the geometry, temperature, and pressure that would enter and exit the nozzle. Using the ideal rocket equations[3], which are located

in the above section, the exit Mach number for the thruster was calculated to be 1.2. The numerical value that resulted from the CFD model indicated that the exit velocity number would be Mach 1.05 which is a 12.5% deviation from the ideal value. However, if the CFD program accounted for the combustion that would take place inside the chamber, the exit Mach number would increase to a value similar to the numerical Mach number. This is known by assuming where both hydrogen and oxygen molecules would merge together and applying another CFD model with the initial temperature being 5025 °F. This model resulted in a max velocity of 5593 ft/s which is equivalent to a Mach number of 1.35. With these results, it is safely to state that the exit velocity of the bipropellant will be around Mach 1.2.

E. **Purchased Component Selection**

A basic functionality diagram was looked at to determine what components would be needed for our gas flow system. The main goal of the design was to make a system as minimal and cost-efficient as possible, while still operating safely and successfully for our needs. Initial iterations determined that a latch valve, followed by a needle valve, followed by a flow meter would be sufficient for the system. Due to budgeting constraints the flow meter was not a viable option and was instead replaced by a piping T and pressure transducer. The final iteration of the system's fluid functionality diagram can be seen in Fig. 11.

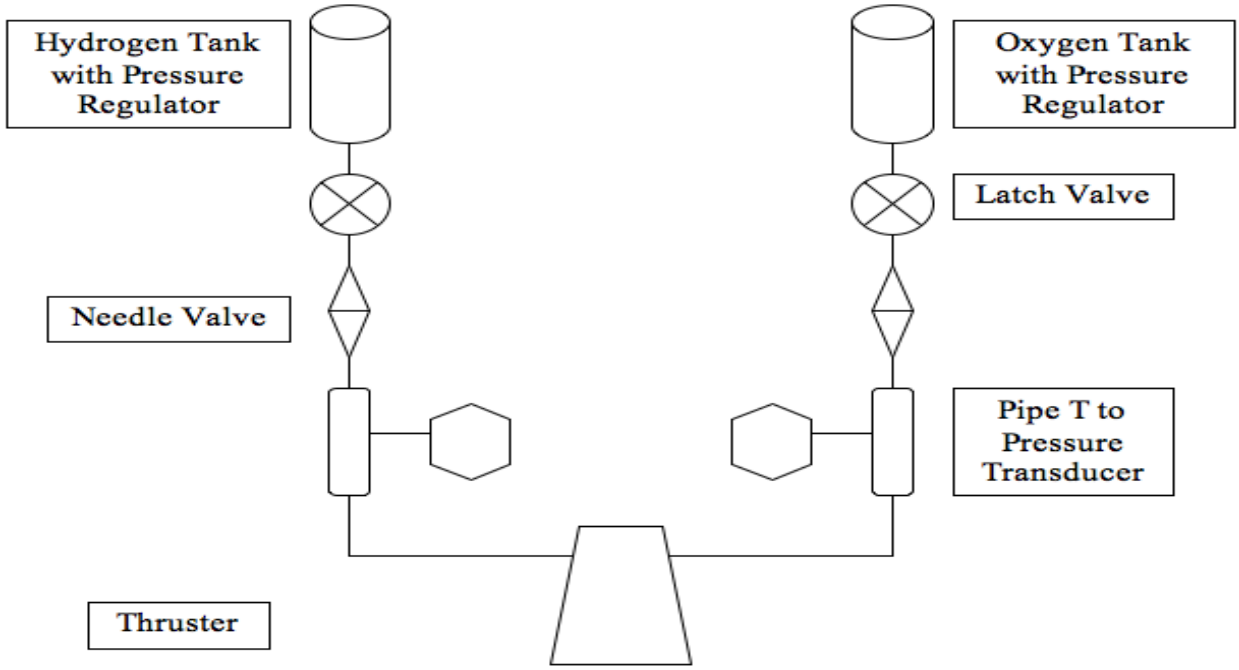

Figure 11:This picture shows how parts and gas flow from tank to the thruster. Tanks have pressure regulators to give the initial pipe pressure, latch valves isolate the system while off, needle valves to fine tune flow and the pressure transducer allows for flow measurements.

All piping was 0.25 in. 316 stainless steel with a 0.016 in. wall thickness. Stainless steel is resistant to corrosion from hydrogen and oxygen and is still workable to allow for bends to be made. The wall thickness of 0.016" was the smallest available while still meeting pressure and safety requirements. The pipes purchased were unthreaded to allow for greater flexibility while assembling. To mate the pipes, Swagelok ¼" 316 stainless steel compression fittings were used. The fittings were compatible with the unthreaded pipe and allowed for the piping system to be assembled and disassembled as necessary

The latch valve was first in line after the tanks because it was necessary to prevent flow from reaching any components before they were ready to be used. This valve had to be able to withstand the required temperatures and pressures of the gases, and needed seals that could stand up to both hydrogen and oxygen corrosion. To fulfill these requirements, a Parker Aerospace normally-closed latch valve was selected. This valve used all stainless steel wetted parts and had 1/4" female NPT fittings that used Pctfe seals.

The needle valve was placed after the latch valve and before the pressure transducer so that gas flow could be fine tuned if necessary. This valve had the same requirements as the latch valve but it's settings had to also be easily

recordable. To fulfill the function of the needle valve an "Easy Set Needle Valve" from McMaster-Carr was used. This valve featured color coding on it's needle handle for easy setting reference, dry seals, 1/4" female NPTF fittings and also had a built in check valve. This check valve gave added protection to the system by not allowing any back pressure to flow back to the latch valve, pressure regulators or tanks.

Last in line before the thruster was the pipe T and pressure transducer. The pressure transducer was used in place of the flow meter by measuring static pressure drop to allow use of Bernoulli's principle to measure volumetric flow rate and a calculated corresponding mass flow rate. The T selected was a Swagelok SS-400-3-4TTF which was a 316 SS construction with two 1/4" compression fittings and one 1/4" female NPT fitting. The Pressure transducer was a Davison A-10 pressure transmitter which featured all stainless steel wetted parts and was designed to measure pressures up to 300 psia.

F. **Pre-Existing Components and Miscellaneous Parts**

Use of as many existing parts as possible was key to staying within budget. Unfortunately, this is a fairly unique project so only a few components could be reused from existing stock. There were 5 primary components used from other projects; the hydrogen tank, oxygen tank, hydrogen regulator, oxygen regulator and the test bed table. These 5 pieces of the test bed would have cost the project over $500, well out of the scope of the projects budget. Other miscellaneous parts such as fasteners, wires, switches and connectors are inexpensive and had no drivers except the test bed requirements, for example voltage and screw thread sizes, so they were a minimal burden on the project budget.

III. Manufacturing

A. **Thruster Machining**

The manufacturing process for the thruster began by extracting dimensions from the CAD model of the chamber and nozzle. Step-by-step handwritten instructions were created as guidelines for the manufacturing process. The instructions were necessary to streamline the machining process, help mitigate cutting mistakes and plan out a feasible manufacturing process. Even if the dimensions needed to be adjusted slightly, the step-by-step handwritten instructions prepared will be the same, just with different numbers. An aluminum prototype was made first to test the chosen manufacturing process and thruster design dimensions. The nozzle and gasket for the final steel design were machined by an outside source to save time.

The first step was to square the thrust chamber, which was done primarily by facing the ends of the aluminum stock flat to avoid measurement errors. After the part was squared, the grooves for the gasket were cut on a face of the chamber. To allow for a better seal the protrusion intended for the gasket on both the thruster chamber and nozzle was changed from 12 thousandths to 20 thousandths.

The next step was to then reduce the diameter from two inches to an inch and a half. A problem encountered was that the remaining flange was not thick enough to provide the stable chuck grip needed to machine the part safely. This problem was solved by using a reverse cutting tool and cutting in the opposite direction leaving the flange. This shows additional time is necessary to prepare for unexpected manufacturing anomalies. For additional strength the flange on the thruster chamber was increased from 0.06 in. to 0.25 in. thick.

The thrust chamber hole was the next feature to be machined. The large diameter was achieved by starting with a small diameter and stepping up with larger drill bits in increments starting at 0.125 in. and stepping up by 0.25 in. The overall diameter could not be perfectly matched by a drill bit available, so the diameter was increased to the next available size which was 0.06875 in. After the chamber hole was finished, the injector holes were drilled using the drill press. The injector holes required a ¼” NPT tap instead of a ¼" tap because the NPT influences the shape of the grooves and under pressure the NPT grooves make a better seal. The 0.4375 in. ignition hole was drilled in the same way as the injector holes and was threaded using a 10mm-1 tap.

The flange holes were then drilled on a mill. A mill was the chosen machine because of the necessary symmetry of the holes. The positions of the holes were mathematically determined in Cartesian coordinates, with the chamber hole being the center, because the mill bit's moved on a flat plane and allowed the bit to move perpendicular to this plane for drilling the holes.

The nozzle was too small of a piece to properly square, so a dial indicator was needed to ensure the part was sitting in the lathe chuck evenly before the initial cuts were made. The facing was similar to facing the chamber, but making the angled nozzle cut required an angled setup and a 0.125 in. diameter long boring bar at least 3” long to cut into the part at the right depth without the thickness of the bar hindering the cut or the lathe chuck crashing

into the part. The boring bar was angled using the fixed marks on the lathe's compound rest and the cut depth was determined using trigonometry compensating for the angled boring bar position.

Machining steps for the steel thruster were identical to the revised aluminum thruster machining with the exception that no spark plug hole was drilled. A different ignition method was chosen after spark plug testing. The stainless steel the cutting depth was changed to 40 thousandths however, as opposed to 30 thousandths for the aluminum, in order to cut below the heat-hardened layer of material from friction. The aluminum was actually more problematic than the stainless steel to manufacture because of the 700 rpm turning speed needing a constant supply of cutting coolant, which the 180 rpm stainless steel did not require. Aluminum also posed some problems being a softer metal which resulted in cuts that were sometimes not as smooth as desired. Overall, the final thruster design deviated little from the initial CAD models. The flange was thickened and the hole diameters were minutely stepped up due to tool availability.

B. **Component and Test Bed Assembly**

The next step of the manufacturing process is to integrate the components selected into one system. The thruster, thruster mount, piping, pressure transducer and valves were to be assembled on top of a movable table. The movable table allowed easy assembly and transportation. The 1/4 in. O.D. stainless steel pipes were cut into 4” long segments that would connect each of the components together via compression fittings. The 4" pipes were long enough to allow some pipe flexibility for mounting errors without pushing components off the edge of the table. These pipes and the valves they connected were laid on the table for positioning. Once component positions were confirmed to be symmetrical, the parts were secured using metal loop straps around the compression fittings. The thruster mount base was attached to the table and then the thruster mount was attached to the base. With the thruster mount assembled and secured the thruster was secured to it's mount. It was now possible to place lines leading from the pressure transducer T to the thruster. These pipes were about 2 ft long each. These lines were bent into a U-shape, as seen in Fig. 12, in order to allow the thruster to rotate about it's hinge with minimal pipe interference. These were bent using a 1/4” pipe bender and were adjusted by hand to properly connect the components to the actual nozzle. Tanks with pressure regulators were placed at the rear of the table where they were to be positioned for testing so pipes could be properly routed from the solenoid to the tank regulators. The last component to be placed was the load cell which was mounted in a small aluminum block to give it the necessary height to reach the base of the thruster mount. The load cell was never secured and was simply placed or removed as necessary to prevent a constant load being placed on it. Repeatability was not an issue because there was only one location where the load cell would properly fit.

Figure 12: This picture shows the bend put into the pipe to allow the thruster to rotate on it's hinge. The other side mirrors the side shown.

IV. Testing

A. Test Apparatus

The testing apparatus of this experiment consisted of two primary parts, control room apparatus and test chamber appraratus. The test chamber apparatus consisted of the test bed which includes the thruster, valves, piping, load cell, pressure transducers, tanks and associated wiring. The test bed held all components except for the tanks on it's surface and was anchored to the ground via tie-down straps. The tanks stood next to the rear of the test bed and were secured to the test bed with a tie down strap. Each electrical unit had wires running to a 12 pin connecter which allowed the test bed to be moved independently of several feet of wire. The opposing side of this connector ran

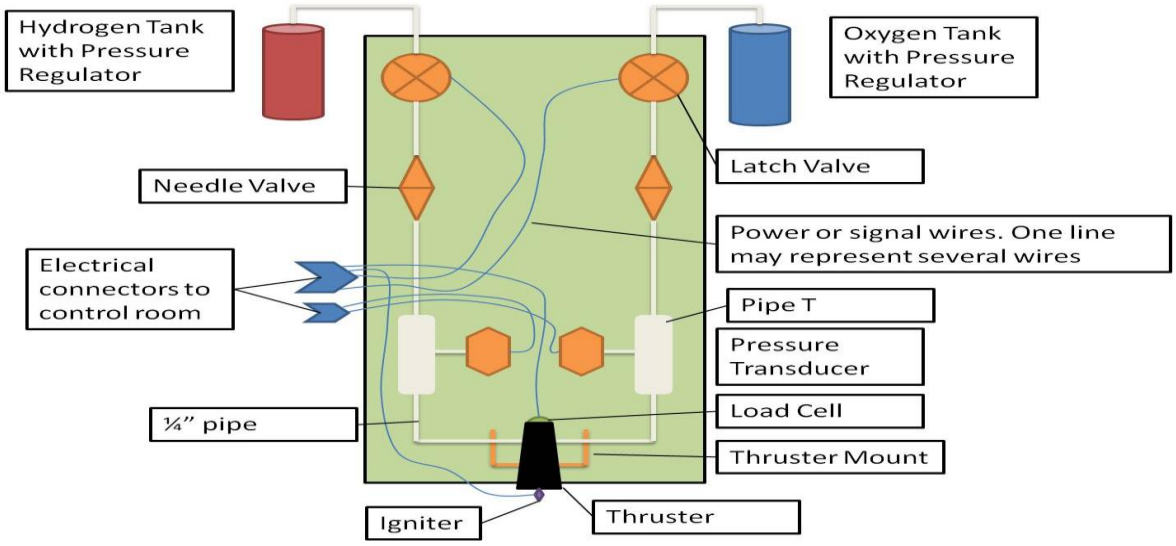

Figure 13: Test chamber apparatus diagram.

wires from the testing chamber to the control room. Figure 13 shows the functionality diagram of the test chamber side of the test apparatus.

The test bed used two devices to control flow, a latch valve and a needle valve. The latch valve was a Parker Aerospace solenoid latch valve operating at 24 V. Each leg of the gas system had it's own dedicated latch and needle valve. These valves shared a common ground and independent positive leads so they could be operated independently while still using a common power supply. A wiring diagram for the latch valves can be seen in Fig. 14. The needle valves were mechanically operated via setting a knob at their top. This valve was set after the

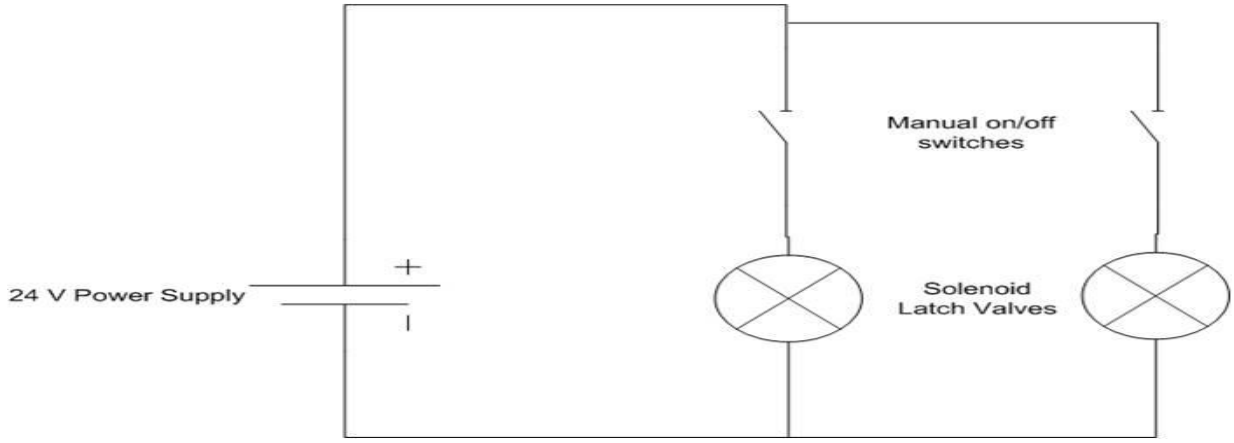

Figure 14: Wiring diagram of the latch valves showing parallel wiring for a shared power supply.

latching valve but before the pressure transducer so that it's affects on flow could be measured. Needle valves were initially set wide open.

The control room apparatus consisted of 4 power supplies, a laptop with LabView, a DAQ board, a multi-meter, a temperature probe and the operational crew. The solenoid valves required one 24 V power supply able to supply at least 1 amp, ignition required one 12 V power supply able to supply at least 1 amp and the pressure transducers required one 30 V power supply each which would not exceed 2 amps. The electrical leads from the test bed led into the control room via a small hole in the wall and allowed the test bed to be powered, monitored and operated safely away from the test bed. The temperature probe was operated before and after firing in the test chamber to ensure that material temperatures were not exceeding safety limitations. Figure 15 shows functionality of the control room side of the test setup.

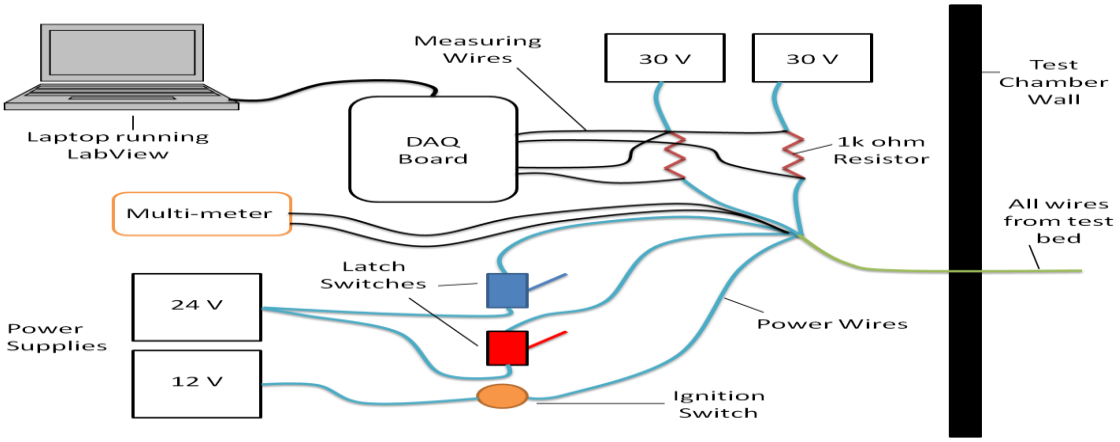

Figure 15: Control room functionality diagram showing where wires split to respective parts.

The testing apparatus used three measuring devices to read live data, two pressure transducers and one load cell. The pressure transducers were operating at 30 V in a two-wire configuration. These transducers are designed to deliver their data via current outputs. Attempts at programming the data acquisition equipment for current measurement were unsuccessful, so instead an alternate circuit configuration was used so potential could be used to measure line pressure. Figure 16 shows the wiring diagram used for the pressure transducers. The load cell was an OMEGA LCFD-25, which is a miniature 25 lbf load cell. This load cell ran at 10 V and output a potential that was measured by a multi-meter. Multiple attempts to measure force through the data acquisition equipment failed, so only steady state and peak values were recorded.

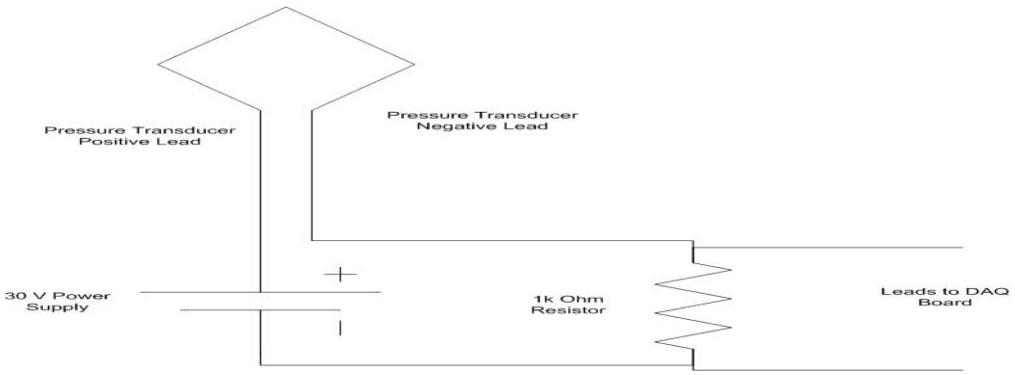

Figure 16: Wiring diagram showing alternative wiring setup used to measure voltage across a resistor instead of measuring transducer current.

LabView was the program used for electronic data acquisition. A VI was programmed to collect pressure data from the two transducers for 20 seconds at a rate of 100 Hz. The VI read in data from the transducers in the form of voltage and passed the values through a function block. This function block contained the calibration equation for the pressure transducers that converted voltage into psig. This function block also had the additional input of a "correction factor" that effectively allowed the output of the function to be shifter up or down so that ambient conditions could read zero. The output of the function block was ran to a waveform chart for live

monitoring and to a data writing block to be recorded for future analysis. Figure 17 shows the LabView dash and Fig. 18 shows the LabView block diagram.

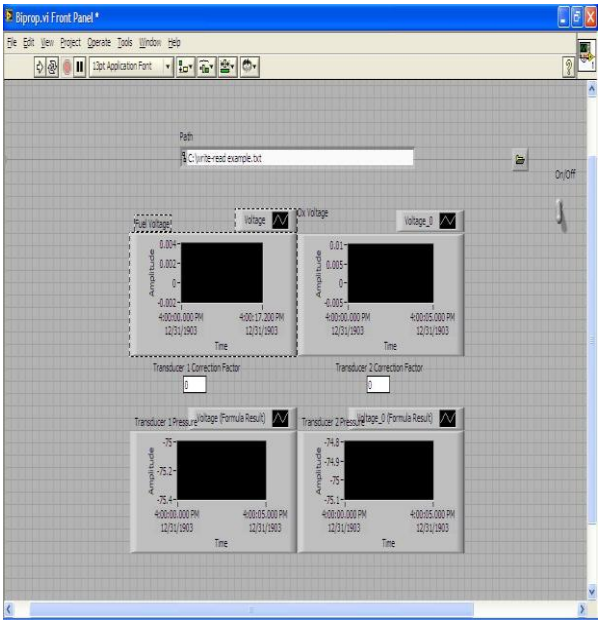

Figure 17: The LabView dashboard shows file directory, transducer voltage graphs, transducer pressure graphs and correction factor inputs.

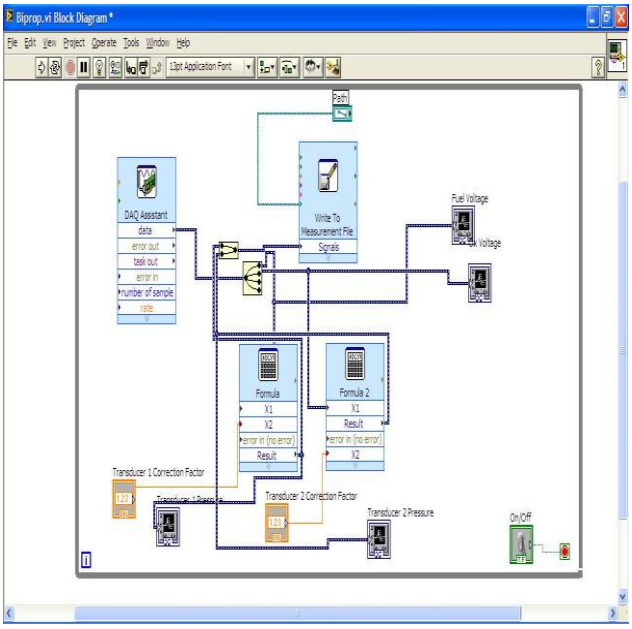

Figure 18: The LabView block diagram shows how data is ran from the DAQ wizard to the graphs, equations and file.

It is notable that no one electronic part shared a common power supply with another with the exception of the two solenoid latch valves. This is because the measuring devices are very sensitive to changes in current or potential caused by the solenoids and there-for had to be separated to prevent any miss-readings that could be caused by this particular form of electrical interference.

B. **Calibration**

The test bed was rolled into Cal Poly's Aerospace Propulsion Laboratory and placed in front of the hybrid rocket test rig with the roller door fully opened. All the control wiring was attached to the test bed, routed into the control room and hooked up as described in the apparatus section. The thruster was removed from the rig, weighed and placed back into it's position. The test bed was then tilted vertically so the the thruster was pointing up as seen in Fig. 19. With the test bed in this orientation, load cell readings were recorded with different weights being placed on to the thruster face to simulate thrust. Load cell readings were then recorded with 0.0, 2.5, 7.5, 12.5 and 17.5 lbf, with an uncertainty of 0.1 lbf, being applied through the thruster's line of thrust. With these points, a calibration curve was created and the test bed was placed back into it's original position.

With the test bed back in it's appropriate orientation, it was anchored down with three tie downs, one pulling back, one pulling forward and left and one pulling forward and right. With the test bed secure, the oxygen tank was rolled to the front of the test bed and attached to what was normally the outlet of the pressure transducer T. This allowed pressure to be applied to the system without leaking out of the thruster. With the tank secured to the test bed, pressures and pressure transmitter voltages were recorded for 0, 40, 60, 80, 100 and 120 psia according to the tank's regulator. With these data points collected the calibration line was created and programmed into the LabView VI so pressure could be recorded live. Only one transducer was calibrated because the transducers have an error of less than 0.25% per the manufacturer test reports and a zeroing factor was programmed into the LabView VI.

Figure 19: This picture shows the test apparatus tilted on it's end with a weight on the thruster for load cell calibration.

The tank valve was closed with the regulator left open, personnel were cleared from the test chamber and the solenoid valve was opened to bleed the oxygen that had built up in the system for calibration. The regulator was then closed, the tanks were placed at their appropriate places at the rear of the test bed, the tanks were secured to the test bed via a tie-down and the transducer T was reattached to it's appropriate line. All piping connections were checked to be tight and secure while personnel took their appropriate places in the control room.

C. **Testing**

At least two people were active during the tests, one person operated LabView and the thruster controls while another recorded load cell data. It was the responsibility of both personnel to monitor burn time. After connections were confirmed to be tight, the regulators were slowly opened to 120 psia for the hydrogen and 122 psia for the oxygen. Personnel were cleared from the test chamber and one at a time the solenoids were opened then closed to ensure that the gases were flowing and that the solenoids were able to completely stop the flow. With the valves confirmed to be good, the rocket igniter has placed into nozzle and it’s power leads were attached. All personnel were moved into the control room and all doors were shut after one person called "Clear" to indicate that the test was about to begin.

To begin the test, the custom LabView VI was started and the thruster was primed by briefly opening and closing both latch valves. The igniter was then lit and aloud to burn for approximately one second before the valves were opened again and the thruster began running. The person monitoring the load cell recorded three data points, nominal voltage before thruster firing, peak value which was typically at thruster start and steady state value during mid operation. Once all values were confirmed to be recorded the valves were closed which ended the thruster firing. The LabView VI was allowed to finish recording it's data points before being shut off and saved. The first test was to confirm that load cell and pressure transducers were operating normally under firing conditions.

While another igniter was being placed, the temperature of the inside of the combustion chamber was measured by placing the temperature probe through the nozzle and leaving it there until it reached it's peak temperature. This temperature, measured before the next run, is labeled as the initial temperature. With the temperature recording complete and new igniter in place, personnel were moved back into the control room. The load cell tare value was recorded, "clear" was called to indicate the start of the test and all doors were shut. With everyone again in place, the lines were primed, the igniter was lit and the valves were opened again to start the

engine. The test was run until all data was confirmed to be recorded at which point the valves and LabView VI were shut off. With the valves confirmed off the temperature probe was placed through the nozzle as quickly as possible to measure combustion chamber post-firing temperature. This value was recorded as final temperature. This process was repeated 2 more times with tank regulator pressures of 80 psia for hydrogen with 82 psia for oxygen and 40 psia for hydrogen with 42 psia for the oxygen. Each time initial temperature, final temperature, line pressures, load cell tare, load cell peak and load cell nominal voltage was recorded.

A fifth and final run was performed to test the hot start capability of the thruster. In this run no data was collected before or during the thruster run. The thruster was ran for approximately 30 seconds and shut off. The thruster was allowed to cool for approximately 5 seconds and then the valves were re-opened. The thruster began firing and was quickly shut off to prevent potential over heating of the thruster. Temperature of the inside of the combustion chamber was recorded as quickly as possible, noted and one more hot-fire test was attempted after all personnel had been moved back inside and "clear" was called. This hot restart attempt failed and concluded the testing of the thruster.

To begin disassembly of the apparatus, the main tank valves were shut, all personnel cleared of the test chamber and the valves were opened to bleed remaining gasses in the lines. With all the gasses confirmed to be cleared, the regulators were then closed and disassembly of the apparatus could begin. The tanks were first released, detached and rolled away. All power supplies were shut down, all wires disconnected and passed back into the test chamber. The test bed was then unanchored and all equipment was loaded and returned to their appropriate locations.

V. Data Processing

In the previous sections, theoretical thruster performance was calculated using the ideal rocket equation. Using the collected data the results of the ideal rocket equations, such as mass flow, thrust and specific impulse, can be compared to experimental results. Calculations began by first taking calibration points for line pressure and load cell force and creating fit curves for each. Curve fits were linear per factory recommendations and resulted in Eq. 14 and Eq. 15,

$$P = 19.156V_{PT} - 73.333 \tag{14}$$

$$F = 3976.2V_{LC} - 627.08 \tag{15}$$

where P is line pressure in psig, V_{PT} is pressure transducer voltage in V, F is load cell force in lbf and V_{LC} is load cell voltage in mV. Due to the fact that the load cell was sensitive and had an initial tare value force on it inherent from the testing rig, calculation of force produced by the thruster deamed to be the most critical, and therefore it was calculated first. Thrust force can be calculated by equation 16,

$$T = F_{measured} - F_{Tare} \tag{16}$$

where $F_{measured}$ is the measured force in lbf, F_{Tare} is the tare force value of the load cell in lbf and T is the thruster output in lbf. Knowing pressure in the lines, gas density could be calculate using an altered ideal gas law as seen in eq. 17,

$$\rho = \frac{144P}{1728RT} \tag{17}$$

where ρ is density in slugs/in^3, R is the gas constant of hydrogen or oxygen in ft-lbf/slug-R and T is temperature of the gas in R. With line pressure and density calculated, mass flow could be calculated using a modified Bernoulli's equation as seen in Eq. 18,

$$\dot{m} = \rho A\sqrt{\frac{2(P1-(P+14.7))}{\rho}} \tag{18}$$

where A is the area of the pipe in in^2, P1 is the regulator pressure in psia and $\dot{m}$ is the mass flow of the gas in slugs/s. One method of judging thruster performance and efficiency is calculating ISP which can be done with Eq. 19,

$$\mathrm{ISP} = \frac{\mathrm{T}}{\dot{\mathrm{m}}_{\mathrm{tot}}\mathrm{g}} \tag{19}$$

where $\dot{m}_{tot}$ is the combined mass flow of hydrogen and oxygen in slugs/s, T is thrust in lbf, g is the acceleration of gravity in ft/s^2 and ISP is thruster specific impulse in s.

VI. Results and Discussion

The mass flow rate was calculated by recording the line pressures with LabView and Eq.s 14, 17 and 18. Matlab was used to generate graphs for the pipe mass flow rates. Figures 20 and 21 represent the first test at 120 psi. The first observation to be noted about these graphs is the noise of the data. The test chamber has had known issues with electro-magnetic interference causing readings dependant on voltage to vary. The two larger spikes at the beginning of the run are not interference but are multiple priming attempts to get the engine started. Once the engine had started, it is interesting to note a slow drop in mass flow as the engine ran. This is indicative of a pressure build up within the combustion chamber feeding back into the lines, slowing the mass flow rate of the gasses. While mass flow was changing, load cell output was not. A combination of these observations suggests that throat area may have reduced as the thruster rapidly heated up and expanded which constricted mass flow.

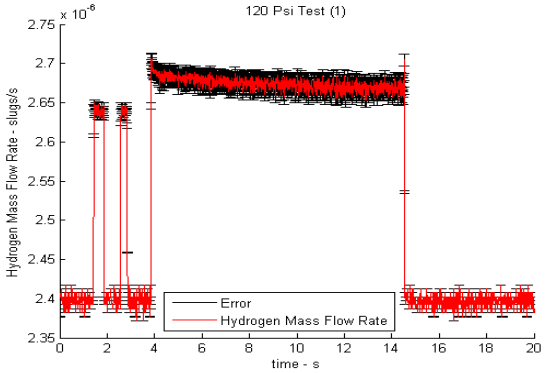

Figure 20: This graph shows hydrogen mass flow for the first 120 psi test with the calculated 2.916% error.

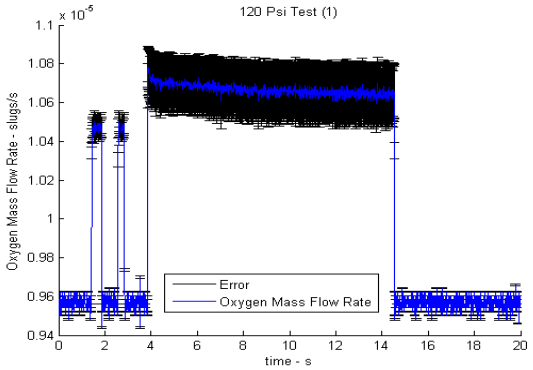

Figure 21: This graph shows oxygen mass flow for the first 120 psi test with the calculated 2.896% error.

Figures 22 and 23 represent the second test at 120 psi. These graphs show similar profiles to test 2 showing consistency in thruster operation and suggesting no immediate degradation of the nozzle. Figures 24 and 25 shows the error between the mass flows for the first and second run showing peak error of 10%. Considering the noise of the data, this is an acceptable difference.

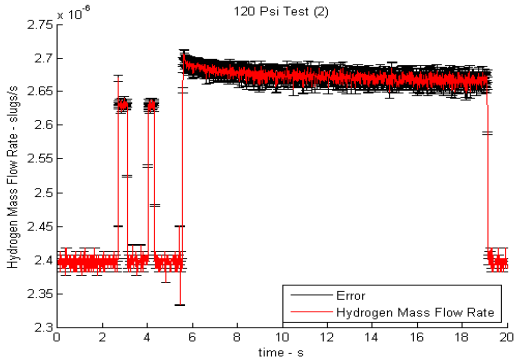

Figure 22: This graph shows hydrogen mass flow for the second 120 psi test with the calculated 2.916% error.

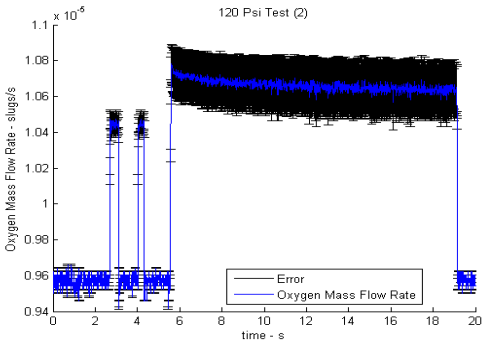

Figure 23: This graph shows oxygen mass flow for the second 120 psi test with the calculated 2.896% error.

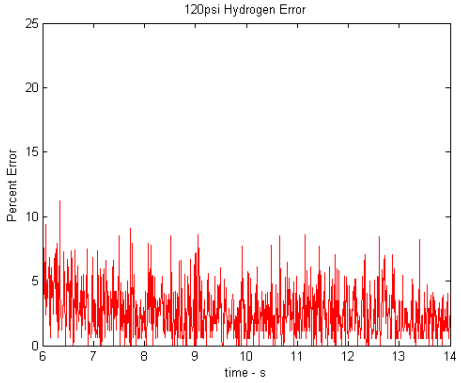

Figure 24: Graph showing error in hydrogen mass flow between the first and second 120 psi runs.

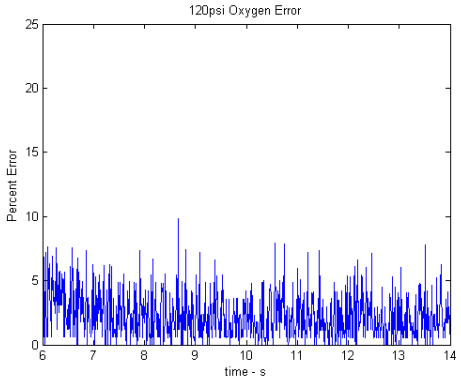

Figure 25: Graph showing error in oxygen mass flow between the first and second 120 psi runs.

Figures 26 and 27 represent the test at 80 psi. Note that there is only one initial spike due to only one ignition attempt. The mass flow for the hydrogen and oxygen drops for this lower pressure run as expected indicating a reduced difference in chamber and regulator pressure.

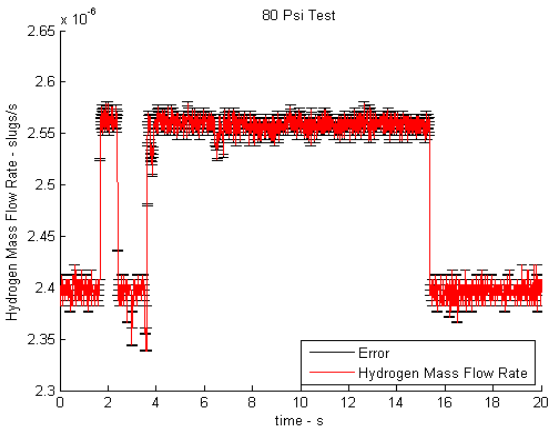

Figure 26: This graph shows hydrogen mass flow for the 80 psi test with the calculated 2.916% error.

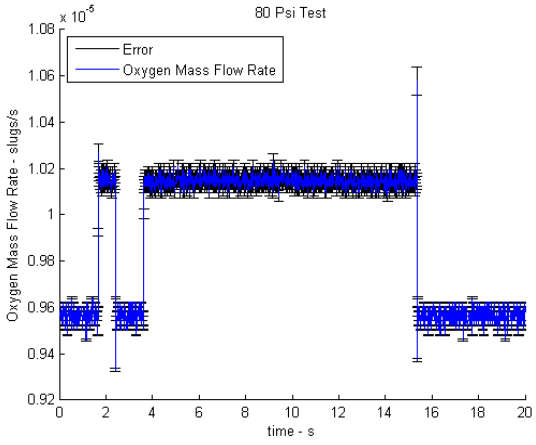

Figure 27: This graph shows oxygen mass flow for the 80 psi test with the calculated 2.896% error.

Figures 28 and 29 represent the test at 40 psi, these graphs again indicate a reduced mass flow rate compared to the higher pressure tests which is consistent with expected trends. This test however shows an interesting phenomenon in the oxygen mass flow rate, it is slowly rising through the duration of the test. This change in mass flow should have changed the mixture ratio of the fuel and oxidizer which should have resulted in a change in force by causing an increase or decrease in combustion efficiency as well as over all mass output. However no changes in force were observed.

Results of mass flow measurements for these experiments showed expected trends but did not follow expected values. Steady state mass flow rate of hydrogen and oxygen for the 120 psi test were expected to be $9.7*10^{-5}$ slugs/s and $7.76*10^{-4}$ slugs/s respectively where experiments shows an average of $2.55*10^{-7}$ slugs/s and $1.1*10^{-6}$ slugs/s with their respective tare values subtracted. Experimental values indicate mass flow rates for hydrogen and oxygen to be several orders of magnitude less than what was calculated. In addition, this also indicates that the mixture ratio was off by a factor of 2. The caveat to these observations is that measurements were based on Bernoulli's principle which has many assumptions such as ideal gasses, incompressible flow and limited correction for flow turbulence. It is suspect that Eq. 5 did not properly account for any extra losses that occurred in the pipes that resulted from turbulence, bends or other flow phenomena. It is also now suspected that hydrogen and oxygen properties are too far from ideal gasses, in terms of compressibility, for Bernoulli's equations to be as accurate as desired.

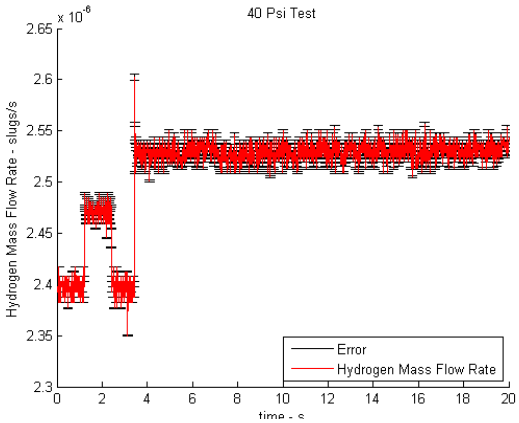

Figure 28: This graph shows hydrogen mass flow for the 80 psi test with the calculated 2.916% error.

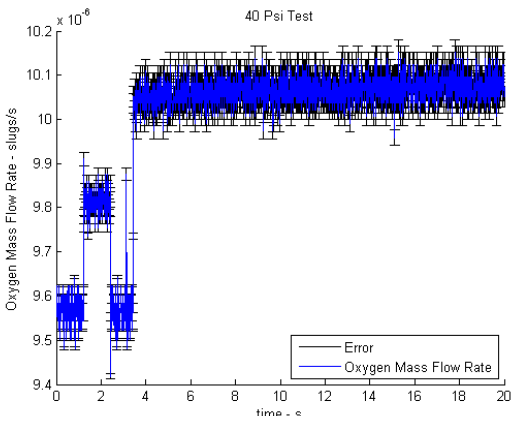

Figure 29: This graph shows hydrogen mass flow for the 80 psi test with the calculated 2.896% error.

The outputs of the load cell were recorded as voltages during the tests and then converted to forces via the load cell calibration curve. The tare compensated for the weight of the thruster and the bending pipe force on the load cell. The nominal steady and nominal peak forces recorded had the tare forces subtracted from them and are displayed in Table 2. It can be seen that measured thrust values were less than what was expected and show unexpected variations from predictions. First, test 1 shows a thruster output at about half of what was expected. Second, test 1 and test 2 results vary despite having the same mass flow rates. Last, test 4 shows a greater thrust value over test 3 despite having a lower inlet pressure. A phenomena to note is varying tare values, which may be cause for the unexpected force values. The system was designed to have the pipes biased down towards the load cell so that they would absorb as little of the thruster force as possible, but if the pipes were not set consistently, it is possible that the thruster was not allowed to press on the load cell consistently. It is clear that this design philosophy has it's flaws and needs to be corrected in future experiments. In addition to this design flaw, the fact that calculations are based on ideal assumptions needs to be also considered. The ideal rocket equations do not account for flow turbulence, imperfect combustion and varying gas properties. The measured mass flows deviating from expected values also suggest that there was variation in mass flow and mixture ratio. Mass flow being measured lower than expected could account for part of the unexpected thrust values. More importantly, the varying mass flows show mixture ratios varying from ideal which could have greatly impacted thruster performance. Running the thruster lean or rich would cause gasses to not expand as expected due to incomplete combustion.

Table 2. This table displays the force results from the load cell for the four measured tests.

	Test 1	Test 2	Test 3	Test 4
Tare Force, lbf	3.55	0.76	5.60	6.79
Measured Force, lbf	5.93	1.96	5.20	6.0
Thrust, lbf	2.38	1.2	0.40	0.79

The specific impulse was calculated using the mass flow rate values drawn from the MATLAB graphs and the force values from the load cell. Test 1 yielded an ISP of 86.0 s, test 2 yielded an ISP of 43.0 s, test 3 yielded an ISP of 0 s and test 4 yielded an ISP of 30.5 s. Values again greatly deviate from the expected 176.63 s but because ISP is dependent on thrust and mass flow values, which have thus far been discovered to be inaccurate, this deviation is expected. However, with the exception of the phenomena of a calculated ISP of 0 s for test 3, the trend is for ISP to drop as force drops. This is expected because the drop in thruster output is greater than the drop in mass flow output causing equation 19 to yield a lower ISP.

One final test was conducted in which no measurements but temperature was considered. This test was to observe the ability of the thruster to hot start, or light without an outside ignition source. The thruster was able to reignite after it's long burn and a rest of approximately 5 seconds without the use of the igniter. Measurements taken after the first hot fire test showed combustion chamber temps in excess of 1100 F while the auto-ignition temperature of hydrogen is 1085 F. This test shows that the thruster is able to withstand temperatures greater than auto-ignition. This means that the use of auto-ignition in hydrogen thrusters is possible though many factors, such as thruster size and environment, will determine the length of time allowed between firing.

VII. Conclusion

The main objective of this project was to gain experience in the process of designing and testing a bipropellant thruster with the added requirement of making the fuels green. Oxygen and hydrogen gas were chosen to be ideal fuels for this project and would easily be able to meet the 5 lbf force requirements for the thruster. The designing and manufacturing process of the project proved to be successful. Calculations using the ideal rocket equations and stress equations agreed with the CFD and FEA models and the thruster was successfully manufactured without incident using a planned process. The testing portion of the project however suffered several complications and failures. Primary flaws in testing lied in too rigid of pipe connections to the thruster and inaccurate flow calculation methods due to incorrect assumptions. Future experiments may try swapping the thruster connection lines with flexible braided hoses, attempting to use a more refined flow calculation method and possibly a secondary flow measuring system to confirm that mass flow measurements are correct. Although the collection of results was not as desired, the process of designing and planning the tests was a vital and successful learning experience.

Difficulty was often encountered in finding simple conceptual answers to questions that is often available in the classroom setting. This project forced the team to exercise not just the calculations learned in class, but the problem solving skills that have been built through the classes. It was discovered that when in doubt, the value of basic experiments and calculations from the engineering fundamentals are valuable for general guidance but a much more detailed analysis is required to match real world results.

Safety was, and continues to be, of utmost importance in the projects performed at Cal Poly. Every component designed and built has met or exceeded safety requirements and the lack of component failures testifies to the safety philosophies adopted in the design. These efforts towards safety as well as a compiled list of the associated risks and how they are mitigated was what enabled this faultless safety record.

It is the hopes of this team that this project sees further research to optimize and mitigate various problems that were encountered and that the lessons learned in this project can assist future projects.

Acknowledgments

The project group would like to first thank Cody Thompson for his assistance in setting up the experiments and machining the steel nozzle for the thruster. The group would also like to thank Dr. Jameson for her guidance and support in the group's efforts.

References

[1] Muller, S. Tomas., "Astrium an EADS Company," *European Space Company's Activites* [online database], URL: http://www.astrium.eads.net/ [cited 16 January 2011].

[2] "Pratt & Whitney is a world leader in the design, manufacture and service of aircraft engines, space propulsion systems and in dustrial gas turbines," *United Technologies Company* [online database], URL: http://www.pw.utc.com/about_us/contact_us.asp [cited 23 January 2011].

[3] Sutton, P. George. and Biblarz, Oscar., "Rocket Propulsion Elements," Wiley-Interscience Publication, John Wiley & Sons Inc., published 2002.

[4] Burkhardt, Holger et al. "Comparative Study of Kerosene and Methane Propellant Engines for Reusable Liquid Booster Stages Holger." (2002): n. pag. Web.

[5] Haeseler, D et al. "Green Propellant Propulsion Concepts for Space Transportation and Technology Needs." NASA Astrophysics Data System (2004): 9. Print.

[6] Kushnir, Peter. "Hydrogen As an Alternative Fuel." *Army Logistics University* June 2000. Web. 8 Mar. 2011.

[7] M.S.C Software Corparation., "NAS120 Analysis Using M.S.C Nastran and M.S.C Patran," Macarthur Place Volume 2., published November 2003.

Appendix

A. **Sample Calculations for Design**

Exit Area (A_e)

$$A_e = A_t * \frac{\left(\left(\frac{(\gamma+1)}{2}\right)^{-\left(\frac{2(\gamma+1)}{(\gamma-1)}\right)}\right)}{M_e * \left(1 + {M_e}^2 * \left(\frac{(\gamma+1)}{2}\right)^{\left(\frac{2(\gamma+1)}{(\gamma-1)}\right)}\right)}$$

$$A_e = 4.8773 * 10^{-4} * \frac{\left(\left(\frac{(1.4+1)}{2}\right)^{-\left(\frac{2(1.4+1)}{(1.4-1)}\right)}\right)}{1.2 * \left(1 + 1.2^2 * \left(\frac{(1.4+1)}{2}\right)^{\left(\frac{2(1.4+1)}{(1.4-1)}\right)}\right)}$$

$$A_e = 5.0374 * 10^{-4} \quad ft^2$$

Throat Pressure (P_t)

$$P_t = \frac{P_e}{\left(\left(1 + \frac{(\gamma-1)}{2}\right){M_e}^2\right)^{\left(\frac{-\gamma}{\gamma-1}\right)}}$$

$$P_t = \frac{4.2609 * 10^3}{\left(\left(1 + \frac{(1.4-1)}{2}\right)1.2^2\right)^{\left(\frac{-1.4}{1.4-1}\right)}}$$

$$P_t = 9.7871 * 10^3 \quad psf$$

Chamber Pressure (P_c)

$$P_c = \frac{P_t}{\left(1 + \frac{(\gamma-1)}{2}\right)^{\left(\frac{-\gamma}{\gamma-1}\right)}}$$

$$P_c = \frac{9.7871 * 10^3}{\left(1 + \frac{(1.4-1)}{2}\right)^{\left(\frac{-1.4}{1.4-1}\right)}}$$

$$P_c = 1.7696 * 10^4 \quad psf$$

Throat Temperature (T_c)

$$T_t = \frac{T_c}{\left(1 + \frac{(\gamma-1)}{2}\right)}$$

$$T_t = \frac{5326}{\left(1 + \frac{(1.4-1)}{2}\right)}$$

$$T_t = 4.7133 * 10^3 \quad °R$$

Exit Temperature (T_e)

$$T_e = \frac{T_t}{\left(1 + \frac{(\gamma - 1)}{2} * {M_e}^2\right)}$$

$$T_e = \frac{4.7133 * 10^3}{\left(1 + \frac{(1.4 - 1)}{2} * 1.2^2\right)}$$

$$T_e = 3.9701 * 10^{\,3}\ \ °R$$

Exit Velocity (V_e)

$$V_e = M_e * \sqrt{\gamma * R * T_e}$$

$$V_e = 4.4588 * 10^3 \quad \frac{ft}{s}$$

Mass flow rate ($\dot{m}$)

$$\dot{m} = \left(\frac{A_t * P_t}{\sqrt{T_t}}\right) * \sqrt{\frac{\gamma}{R}} * \left(\frac{(\gamma + 1)}{2}\right)^{-\left(\frac{\gamma+1}{(\gamma-1)*2}\right)}$$

$$\dot{m} = \left(\frac{4.8773 * 10^{-4} * 9.7871 * 10^3}{\sqrt{4.7133 * 10^3}}\right) * \sqrt{\frac{1.4}{2760}} * \left(\frac{(1.4 + 1)}{2}\right)^{-\left(\frac{1.4+1}{(1.4-1)*2}\right)}$$

$$\dot{m} = 8.7341 * 10^{-4} \quad \frac{slugs}{s}$$

Force (F)

$$F = \dot{m} * V_e + (P_e - P_a) * A_e$$

$$F = 8.7341 * 10^{-4} * 4.4588 * 10^3 + (4.2609 * 10^3 - 2.1304 * 10^3) * 5.0374 * 10^{-4}$$

$$F = 4.9675\ lbf$$

Specific Impulse (Isp)

$$Isp = \frac{F}{(g * \dot{m})}$$

$$Isp = \frac{4.9675}{(32.2 * 8.7341 * 10^{-4})}$$

$$Isp = 176.632\ s$$

B. **Experimental Error Analysis**

Error for Pressure Converter (P)

$$\mathrm{P} = 19.156\mathrm{V_{PT}} - 73.333$$

$$\delta P = \sqrt{\left(\frac{\delta P}{\delta \mathrm{V_{PT}}}\right)^2}$$

$$\frac{\delta P}{P} = \sqrt{\frac{\delta P^{\,2}}{\mathrm{V_{PT}}}}$$

$$\frac{dP}{P} = \sqrt{\frac{d\mathrm{V_{PT}}^{\,2}}{\mathrm{V_{PT}}}}$$

$$\frac{dP}{P} = \sqrt{\frac{.0025\ volts^2}{4.679\ volts}}$$

$$\frac{dP}{P} = 0.0005343 = 0.0534\%$$

Error for Force Converter (F)

$$F = 3976.2V_{LC} - 627.08$$

$$\delta F = \sqrt{\left(\frac{\delta F}{\delta V_{LC}}\right)^2}$$

$$\frac{\delta F}{F} = \sqrt{\frac{\delta F}{V_{LC}}^2}$$

$$\frac{dF}{F} = \sqrt{\frac{dV_{LC}}{V_{LC}}^2}$$

$$\frac{dF}{F} = \sqrt{\frac{.001\ volts}{.1592\ volts}^2}$$

$$\frac{dF}{F} = 0.00628 = 0.628\%$$

Error for Oxygen Pressure Regulator (O_{P_1})

$$\frac{\delta O_{P_1}}{O_{P_1}} = \sqrt{\left(\frac{\delta O_{P_1}}{O_{P_1}}\right)^2}$$

$$\frac{\delta O_{P_1}}{O_{P_1}} = \frac{\delta O_{P_1}}{O_{P_1}}$$

$$\frac{dO_{P_1}}{O_{P_1}} = \frac{dO_{P_1}}{O_{P_1}}$$

$$\frac{dO_{P_1}}{O_{P_1}} = \frac{2\ psia}{121\ psia}$$

$$\frac{dO_{P_1}}{O_{P_1}} = 0.01652 = 1.652\%$$

Error for Hydrogen Pressure Regulator (H_{P_1})

$$\frac{\delta H_{P_1}}{H_{P_1}} = \sqrt{\left(\frac{\delta H_{P_1}}{H_{P_1}}\right)^2}$$

$$\frac{\delta H_{P_1}}{H_{P_1}} = \frac{\delta H_{P_1}}{H_{P_1}}$$

$$\frac{dH_{P_1}}{H_{P_1}} = \frac{dH_{P_1}}{H_{P_1}}$$

$$\frac{dH_{P_1}}{H_{P_1}} = \frac{2\ psia}{120\ psia}$$

$$\frac{dH_{P_1}}{H_{P_1}} = 0.01666 = 1.666\%$$

Error for Thrust Difference (T)

$$T = F_{measured} - F_{Tare}$$

$$(\Delta T) = [(\Delta F)_{measured} - (\Delta F)_{tare}]$$

$$\delta(\Delta T) = \sqrt{\left(\frac{\partial(\Delta T)}{\partial(\Delta F)_{measured}}\delta(\Delta F)_{measured}\right)^2 + \left(\frac{\partial(\Delta T)}{\partial(\Delta F)_{tare}}\delta(\Delta F)_{tare}\right)^2}$$

$$\delta(\Delta T) = \sqrt{(\delta(\Delta F)_{measured})^2 + (\delta(\Delta F)_{tare})^2}$$

$$d(\Delta T) = \sqrt{(d(\Delta F)_{measured})^2 + (d(\Delta F)_{tare})^2}$$

$$\frac{d(\Delta T)}{(\Delta T)} = \frac{1}{(\Delta T)}\sqrt{(d(\Delta F)_{measured})^2 + (d(\Delta F)_{tare})^2}$$

$$\frac{d(\Delta T)}{(\Delta T)} = \sqrt{\left(\frac{d(\Delta F)_{measured}}{(\Delta F)_{measured}}\right)^2 + \left(\frac{d(\Delta F)_{tare}}{(\Delta F)_{tare}}\right)^2}$$

$$\frac{d(\Delta T)}{(\Delta T)} = \sqrt{\left(\frac{0.00628\ lbs}{5.93\ lbs}\right)^2 + \left(\frac{0.00628\ lbs}{3.55\ lbs}\right)^2}$$

$$\frac{d(\Delta T)}{(\Delta T)} = 0.002061 = 0.2061\%$$

Error for Hydrogen Density (ρ_H)

$$\rho_H = \frac{144 H_{P_1}}{1728 RT}$$

$$\delta\rho_H = \sqrt{\left(\frac{\partial\rho_H}{\partial H_{P_1}}\delta H_{P_1}\right)^2 + \left(\frac{\partial\rho_H}{\partial R}\delta R\right)^2 + \left(\frac{\partial\rho_H}{\partial \mathrm{T}}\delta \mathrm{T}\right)^2}$$

$$\delta\rho_H = \sqrt{\left(\frac{1}{RT}\delta H_{P_1}\right)^2 + \left(\frac{H_{P_1}}{\mathrm{T}}\delta R\right)^2 + \left(\frac{H_{P_1}}{\mathrm{R}}\delta \mathrm{T}\right)^2}$$

$$\delta\rho_H = \sqrt{\left(\frac{H_{P_1}}{RT}\right)^2\left[\left(\frac{\delta H_{P_1}}{\mathrm{P}}\right)^2 + \left(\frac{\delta R}{R}\right)^2 + \left(\frac{\delta \mathrm{T}}{\mathrm{T}}\right)^2\right]}$$

$$\frac{\delta\rho_H}{\rho_H} = \sqrt{\left(\frac{\delta H_{P_1}}{H_{P_1}}\right)^2 + \left(\frac{\delta R}{R}\right)^2 + \left(\frac{\delta \mathrm{T}}{\mathrm{T}}\right)^2}$$

$$\frac{\delta\rho_H}{\rho_H} = \sqrt{(0.01666)^2 + (0.00004)^2 + (0.00187)^2}$$

$$\frac{\delta\rho_H}{\rho_H} = .016705 = 1.6705\%$$

Error for Oxygen Density (ρ_O)

$$\rho_O = \frac{144 O_{P_1}}{1728 RT}$$

$$\delta\rho_O = \sqrt{\left(\frac{\partial\rho_O}{\partial O_{P_1}}\delta O_{P_1}\right)^2 + \left(\frac{\partial\rho_O}{\partial R}\delta R\right)^2 + \left(\frac{\partial\rho_O}{\partial \mathrm{T}}\delta \mathrm{T}\right)^2}$$

$$\delta\rho_O = \sqrt{\left(\frac{1}{RT}\delta O_{P_1}\right)^2 + \left(\frac{O_{P_1}}{\mathrm{T}}\delta R\right)^2 + \left(\frac{O_{P_1}}{\mathrm{R}}\delta \mathrm{T}\right)^2}$$

$$\delta\rho_O = \sqrt{\left(\frac{O_{P_1}}{RT}\right)^2\left[\left(\frac{\delta O_{P_1}}{\mathrm{P}}\right)^2 + \left(\frac{\delta R}{R}\right)^2 + \left(\frac{\delta \mathrm{T}}{\mathrm{T}}\right)^2\right]}$$

$$\frac{\delta\rho_O}{\rho_O} = \sqrt{\left(\frac{\delta O_{P_1}}{O_{P_1}}\right)^2 + \left(\frac{\delta R}{R}\right)^2 + \left(\frac{\delta \mathrm{T}}{\mathrm{T}}\right)^2}$$

$$\frac{\delta\rho_O}{\rho_O} = \sqrt{(0.01652)^2 + (0.0006)^2 + (0.00187)^2}$$

$$\frac{\delta\rho_O}{\rho_O} = .0166 = 1.663\%$$

Error for Oxygen Mass Flow Rate ($\dot{m}_o$)

$$\dot{m}_o = \rho_O A\sqrt{\frac{2\left(O_{P_1} - (P)\right)}{\rho_O}}$$

$$\delta\dot{m}_o = \sqrt{\left(\frac{\partial\dot{m}_o}{\partial\rho_O}\delta\rho_O\right)^2 + \left(\frac{\partial\dot{m}_o}{\partial A}\delta A\right)^2 + \left(\frac{\partial\dot{m}_o}{\partial O_{P_1}}\delta O_{P_1}\right)^2 + \left(\frac{\partial\dot{m}_o}{\partial P}\delta P\right)^2 + \left(\frac{\partial\dot{m}_o}{\partial\rho_O}\delta\rho_O\right)^2}$$

$$\delta\dot{m}_o = \sqrt{\begin{aligned}&\left(A\sqrt{\frac{\left(O_{P_1} - (P)\right)}{\rho_O}}\delta\rho_O\right)^2 + \left(\rho_O\sqrt{\frac{\left(O_{P_1} - (P)\right)}{\rho_O}}\delta A\right)^2 + \left(\rho_O A\sqrt{\frac{\left(-(P)\right)}{\rho_O}}\delta O_{P_1}\right)^2 + \left(\rho_O A\sqrt{\frac{\left(O_{P_1}\right)}{\rho_O}}\delta P\right)^2 \\ &+ \left(\rho_O A\sqrt{O_{P_1} - (P)}\delta\rho_O\right)^2\end{aligned}}$$

$$\delta\dot{m}_o = \sqrt{\left(\rho_O A\sqrt{\frac{\left(O_{P_1} - (P)\right)}{\rho_O}}\right)^2\left[\left(\frac{\delta\rho_O}{\rho_O}\right)^2 + \left(\frac{\delta A}{A}\right)^2 + \left(\frac{\delta O_{P_1}}{O_{P_1}}\right)^2 + \left(\frac{\delta P}{P}\right)^2 + \left(\frac{\delta\rho_O}{\rho_O}\right)^2\right]}$$

$$\frac{\delta\dot{m}_o}{\dot{m}_o} = \sqrt{\left(\frac{\delta\rho_O}{\rho_O}\right)^2 + \left(\frac{\delta A}{A}\right)^2 + \left(\frac{\delta O_{P_1}}{O_{P_1}}\right)^2 + \left(\frac{\delta P}{P}\right)^2 + \left(\frac{\delta\rho_O}{\rho_O}\right)^2}$$

$$\frac{\delta\dot{m}_o}{\dot{m}_o} = \sqrt{(.0166)^2 + (0.003484)^2 + (0.01652)^2 + (0.0005343)^2 + (.01667)^2}$$

$$\frac{\delta\dot{m}_o}{\dot{m}_o} = .02896 = 2.896\%$$

Error for Hydrogen Mass Flow Rate ($\dot{m}_H$)

$$\dot{m}_H = \rho_H A\sqrt{\frac{2\left(H_{P_1} - (P)\right)}{\rho_H}}$$

$$\delta\dot{m}_H = \sqrt{\left(\frac{\partial\dot{m}_H}{\partial\rho_H}\delta\rho_H\right)^2 + \left(\frac{\partial\dot{m}_H}{\partial A}\delta A\right)^2 + \left(\frac{\partial\dot{m}_H}{\partial H_{P_1}}\delta H_{P_1}\right)^2 + \left(\frac{\partial\dot{m}_H}{\partial P}\delta P\right)^2 + \left(\frac{\partial\dot{m}_H}{\partial\rho_H}\delta\rho_H\right)^2}$$

$$\delta\dot{m}_H = \sqrt{\begin{aligned}&\left(A\sqrt{\frac{\left(H_{P_1} - (P)\right)}{\rho_H}}\delta\rho_H\right)^2 + \left(\rho_H\sqrt{\frac{\left(H_{P_1} - (P)\right)}{\rho_H}}\delta A\right)^2 + \left(\rho_O A\sqrt{\frac{\left(-(P)\right)}{\rho_H}}\delta H_{P_1}\right)^2 + \left(\rho_H A\sqrt{\frac{\left(H_{P_1}\right)}{\rho_H}}\delta P\right)^2\\&+\left(\rho_H A\sqrt{H_{P_1} - (P)}\delta\rho_H\right)^2\end{aligned}}$$

$$\delta\dot{m}_H = \sqrt{\left(\rho_H A\sqrt{\frac{\left(O_{P_1} - (P)\right)}{\rho_O}}\right)^2\left[\left(\frac{\delta\rho_H}{\rho_H}\right)^2 + \left(\frac{\delta A}{A}\right)^2 + \left(\frac{\delta H_{P_1}}{H_{P_1}}\right)^2 + \left(\frac{\delta P}{P}\right)^2 + \left(\frac{\delta\rho_H}{\rho_H}\right)^2\right]}$$

$$\frac{\delta\dot{m}_H}{\dot{m}_H} = \sqrt{\left(\frac{\delta\rho_H}{\rho_H}\right)^2 + \left(\frac{\delta A}{A}\right)^2 + \left(\frac{\delta H_{P_1}}{H_{P_1}}\right)^2 + \left(\frac{\delta P}{P}\right)^2 + \left(\frac{\delta\rho_H}{\rho_H}\right)^2}$$

$$\frac{\delta\dot{m}_H}{\dot{m}_H} = \sqrt{(.016705)^2 + (0.003484)^2 + (0.01666)^2 + (0.0005343)^2 + (.016705)^2}$$

$$\frac{\delta\dot{m}_H}{\dot{m}_H} = .02916 = 2.916\%$$

Error for Specific Impulse (ISP)

$$ISP = \frac{T}{\dot{m}_{tot}g}$$

$$\delta ISP = \sqrt{\left(\frac{\partial ISP}{\partial\dot{m}_{tot}}\delta\dot{m}_{tot}\right)^2 + \left(\frac{\partial ISP}{\partial T}\delta T\right)^2}$$

$$\delta ISP = \sqrt{\left(\frac{T}{g}\delta\dot{m}_{tot}\right)^2 + \left(\frac{\delta T}{\dot{m}_{tot}g}\right)^2}$$

$$\delta ISP = \sqrt{\left(\frac{T}{\dot{m}_{tot}g}\right)^2\left[\left(\frac{\delta\dot{m}_{tot}}{\dot{m}_{tot}}\right)^2 + \left(\frac{\delta T}{T}\right)^2\right]}$$

$$\frac{\delta ISP}{ISP} = \sqrt{\left(\frac{\delta\dot{m}_{tot}}{\dot{m}_{tot}}\right)^2 + \left(\frac{\delta T}{T}\right)^2}$$

$$\frac{\delta ISP}{ISP} = \sqrt{(.04109)^2 + (0.00628)^2}$$

$$\frac{\delta\eta}{\eta} = 0.04156 = 4.156\%$$